ISOTOPE SHIFT MEASUREMENTS OF THE STABLE KRYPTON ISOTOPES IN NATURAL AND ENRICHED CONCENTRATIONS.

by

© Jacques Dubeau B.Sc.

A thesis submitted to the Faculty of Graduate Studies and Research in partial fulfillment of the degree of Master of Science.

Department of Physics,
McGill University,
Montreal, Canada.

August 1986

ISBN 0-315-38252-X

Abstract

The isotopic shifts of the 587 nm line, corresponding to the transition 5s[3/2]1-5p'[3/2]2, have been measured for the five stable even isotopes of krypton. Also, four hyperfine structure peaks belonging to the stable Kr^{83} isotope have been studied. Two sets of experiments have been done. In the first set, Kr gas containing the stable isotopes in natural abundance has been used. In the second set, mixtures containing highly enriched concentrations of Kr^{78} were used in order to get a reliable measurement of the Kr^{78}-Kr^{80} shift.

Polarisation spectroscopy is the technique used. However, a double probe beam was used, in order to subtract out from the isotope shift spectra the doppler absorption curve. The laser output beam was frequency modulated to reduce the detector noise due to room light and stray reflections of the laser light.

Using previously published shift results pertaining to the 557 nm line, it was possible to separate the field shift contribution from the total shift, and to calculate the change in mean square nuclear charge radius between the isotopes. The results were found to be in agreement with those of previous studies.

Résumé

Les déplacements isotopiques de la raie de 587 nm, correspondant à la transition 5s[3/2]1-5p'[3/2]2, furent mesurés pour les cinq isotopes pairs et stables du krypton. De plus quatre transitions hyperfines du Kr^{83} furent étudiées. Deux séries d'expériences furent accomplies. Dans la première série, du gaz contenant les isotopes de krypton dans leur proportion naturelle fut utilisé. Dans la seconde série, du Kr hautement enrichi en Kr^{78} fut utilisé afin d'obtenir une valeur fiable du déplacement isotopique de la paire Kr^{78}-Kr^{80}.

La technique de spectroscopie de polarisation fut utilisée avec de légères modifications. Deux faisceaux d'échantillonage, l'un servant de signal et l'autre de référence, furent utilisés de façon à réduire la courbe d'absorption tout en conservant le signal de polarisation. De plus le faisceau initial était modulé en fréquence de façon à réduire le bruit dû à la réflection de lumière parasite dans les détecteurs.

Les données expérimentales permirent le calcul de l'effet de volume et des changements du carré moyen de la distribution de la charge nucléaire d'un isotope à l'autre. Les résultats concordent avec ceux obtenus par d'autres chercheurs.

Acknowledgements

First and foremost, I would like to thank Dr. John E. Crawford, my supervisor, who suggested this project and directed me throughout its realisation. I am very much indebted to Daniel Audet, who spent many days introducing me to the technique of polarisation spectroscopy. I wish to thank Dr. Jacques Pinard, of the Aimé Cotton laboratory in Orsay, who proposed the background reducing, frequency modulation technique. I appreciate very much the time and advice he offered me.

I wish to thank also Dr. V. Raut, who introduced me to the mysteries of the dye laser, M. Steve Kecani, who machined greatly needed parts, M. Mario Della Neve, who spent some time working on the vacuum system, and Eric Ramsay, who proof-read this thesis. I wish to thank especially Josée Dubeau, who drew some of the diagrams found in this thesis.

I appreciate the competent help and advice I received from the staff and students of the Foster Radiation Laboratory.

Last but not least, I want to thank Danièle for her encouraging letters.

Table of contents

Table of figures

To my family.

Introduction

In this work, the 587 nm line of krypton, corresponding to the transition 5s[3/2]1-5p'[3/2]2, is studied using polarisation spectroscopy. This way, the isotope shifts of the five even krypton isotopes (A=78 to 86), as well as the hyperfine structure of Kr^{83} will be found. Two sets of experiments were performed. First, laser spectroscopy is done on krypton in natural abundance, yielding the isotope shifts of the four heaviest isotopes, which are also the most abundant. Second, mixtures containing highly enriched amounts of the rare Kr^{78} are used in order to get the Kr^{78}-Kr^{80} shift. Ultimately, the changes in mean square charge radius when two neutrons are added to a Kr nucleus will be found.

The polarisation technique used here contains two important modifications to the one usually described in the literature. First, a double probe laser beam is used, and second, the dye laser output beam is frequency modulated.

This report is divided into four chapters. Chapter 1 is a review of isotopic shift studies, particularly those involving krypton. Then the theory of isotope shift is outlined. In chapter 2, some laser spectroscopic techniques are discussed, a greater part of the chapter being devoted to polarisation spectroscopy. Chapter 3 presents the experimental set-up and technique used, and some of the resulting data. And finally, the analysis of the data is done in the last chapter.

Chapter 1: Isotope shift

1.1) History

1.1.1) History of isotope shifts

Isotope shift refers to the very fine structure observed around a particular line emitted from a mixture of isotopes of a given element. This structure is due to differences in the nuclear masses and mean nuclear charge radius between the isotopes. Measurements of these shifts give valuable information about the mass, the shape and the charge distribution of a nucleus in its ground state, as well as indirect information about the spin and nuclear moments. Typically isotope shifts represent 2.5 ppm of the wavelength and thus could not be observed before the advent of interferometric methods.

In 1890, Michelson [Mic 1893] observed structures down to the order of 0.01 Å in spectral lines. They may have been due to isotope shift (IS) or hyperfine structure (HFS). In 1913, as Bohr's theory of the atom appeared, it was suggested that the electronic energy levels might be mass dependent. It was not until 1918 that the first measurement of an IS was made. Aronberg [Kin 84a] found that radioactive lead emits a photon of wavelength 4.3 mÅ over that of the 4058 Å photon from stable lead.

In 1922 it was found that some IS were too large to be due to nuclear mass effects alone. Ehrenfest [Ehr 22] suggested that another contribution could come from differences in the nuclear structure of different isotopes, which would give a slightly different force field surrounding the nuclei. However, it was not until 1932 that the first quantitative formulation for the field shift was done by Breit, Rosenthal and Racah [Bre 32].

In the 1930's, lasers were still a long way off and enriched isotopes were not available; it was possible to study only isotopes whose IS are large and the lines narrow. Hollow cathode lamps were used and the spectra were observed in high resolution by photographing the fringe pattern produced by a Fabry-Perot etalon. During that time, Jackson and Kuhn [Jac 38] in 1938 were the first to use a Doppler limiting technique. They measured resonance line photons emitted at a right angle from a beam of potassium atoms. The very small transverse velocity component of the atoms contributed little to the broadening of the lines.

In the 1950's some enriched isotopes became available and photomultipliers were developed. Isotope shifts were measured on heavy isotopes; among them, thallium and mercury.

In the very early works on isotope shifts, one sought to determine the field shift contribution in order to extract information on the non-relativistic electronic density at the nucleus, $|\psi(0)|^2$. In the 1960's and up to the

present, isotope shifts were measured in order to get information on the nuclear structure and shape through the determination of the change in the mean square charge distribution $\delta\langle r^2\rangle$ between isotopes. Between 1960 and 1970 lasers were introduced to the field. The accuracy of measurements went from 3 MHz in the best of non-laser work to 300 KHz using lasers. The first isotope shift measurement using lasers was done by Brochard and Vetter [Broc 66] in 1966 on xenon. In 1974 Hansch and Broadhurst [Broa 74] made the first Doppler-free measurement using a tunable dye laser.

Since then, many variations of the Doppler-free techniques have appeared. Studies now are concentrating on isotopes whose neutron numbers are close to a magic number, such as Sr and Kr, and on mass separated short-lived isotopes.

1.1.2) Krypton studies

Measurements of the isotope shift of Kr isotopes is of particular interest. There are five even stable isotopes of Kr ranging in mass number from 78 to 86, the last of which corresponds to the $g_{9/2}$ neutron shell closure. If the field effect contribution to the shift is separated from the total shift, one actually finds a decrease in mean square nuclear charge distribution ($\langle r^2\rangle$) when neutron pairs are added. In this case, one talks about $\delta^{AA'}\langle r^2\rangle$being

negative or reversed.

The following is a brief history of the spectroscopic studies that have already been done on Kr. As of now, IS measurements have been done only on the five stable even isotopes.

The first IS measurements on Kr were made in 1949 by Koch and Rasmussen [Koc 49]. In these measurements, the hfs of Kr^{83} for the 805.9 nm line corresponding to the transition 5s'[1/2]0-5p'[3/2]1 was determined. In order to determine the center of gravity of the splitting, they measured the Kr^{82} and Kr^{84} lines and found a shift of 0.00013 nm. Discharge tubes containing slightly enriched amounts of the two even isotopes were used.

In 1976 Brechignac and Gerstenkorn [Brec 76] did IS measurements of the five even stable Kr isotopes for the 3.066 micrometer infrared line corresponding to 6p[1/2]1-6s[3/2]2. They observed irregular IS which they related to irregular variations of $\langle r^2 \rangle$. Their results hinted at the presence of a volume (or field) effect and the possible inversion of $\delta\langle r^2 \rangle$.

In order to have a sizable field shift it is necessary to examine a transition in which one of the states has a high probability density at the nucleus. Studies were done on transitions which involve a 5s level. This should then show a greater volume effect than the infrared transition. In 1977 Gerhardt and Matthias [Ger 77] studied the 557 nm line using Doppler-free polarisation

spectroscopy, obtaining a large signal due to the presence of a metastable lower level. Their results showed a non-negligible volume effect. Adding neutrons in the lower half of the $g_{9/2}$ shell (N=78 to 80) introduced the largest change in $\langle r^2 \rangle$. The second half of the shell (N=82 to 86) showed a somewhat smaller variation. At that stage one could only show departure of the total shift from that of a pure mass shift. To evaluate explicitly the field shift and $\delta\langle r^2 \rangle$ one had to wait for theoretical studies which were done in 1979. The technique used by Gerhardt and Matthias is also the one used in this work, and will be described in chapter 2.

In 1978 Jackson [Jac 78] used an arc lamp containing highly enriched amounts of the stable isotopes and did IS measurements on 14 IR lines in the 750 A to 800 A region. IS were measured on photographically recorded fringes from a Fabry-Perot etalon. The same year, Champeau and Keller [Cha 78] did a laser excitation study on the 557 nm line, corresponding to the transition 5s[3/2]2-5p'[1/2]1, by using an atomic beam of Kr and detecting the resonance fluorescence. Isotope shifts were measured but a definite trend of the field shift could not be established. Gerhardt [Ger 79] measured in 1979 the IS on the 432 nm and 557 nm lines using again polarisation spectroscopy. At that time F(557), the electronic factor for the 557 nm line had been evaluated and $\delta^{\blacksquare\blacksquare}\langle r^2 \rangle$ had been derived theoretically (the electronic factor of a transition multiplied by the change

in mean square charge distribution between two isotopes gives the field shift). These two estimates enabled the determination of $\delta\langle r^2\rangle$ for any pair of even Kr isotopes. As expected, a decrease in $\langle r^2\rangle$ with increasing mass number throughout the neutron shell was observed. These negative $\delta\langle r^2\rangle$ values were interpreted by Gerhardt as being related to a decrease in nuclear deformation and/or a decrease in skin thickness.

Using the same technique as in 1978, Jackson [Jac 80] in 1980 found that transitions involving a 5p electron display a field shift of the same order as those involving a 5s electron. He worked with the 587 nm line, which is also the one studied in the present work.

In 1985 Audet [Aud 85], using polarisation spectroscopy, and Savard [Sav 85], who used saturation spectroscopy, also studied the 587 nm line and measured the IS between the four most abundant even stable Kr isotopes and the hyperfine structure of Kr^{83}. The shifts were in agreement with the results obtained by Jackson. Their measurements were performed at the Foster Radiation Laboratory at McGill University.

1.2) Theory of isotopic shifts

The isotopic shifts observed in electronic transitions are easily understood if the nucleus is taken as

having a finite mass and non-zero radius rather than being a point of infinite mass. It is then found that the energy of an electronic level does not depend on Z alone but also on the mass (M_A) and on the radial charge distribution of the nucleus. Three effects contribute to the observed shift of a level; they are, the normal mass shift (NMS), the specific mass shift (SMS) and the field shift (FS). They will be treated separately in the following sections.

1.2.1) Normal and specific mass shifts

The Hamiltonian for an atom of infinite nuclear mass is

$$(1.1) \qquad H = \sum_k p_k^2/2m_e + \sum_k (-Z_o/r_k) + \sum_{k<l} 1/r_{kl} \ ,$$

where the symbols have their usual meaning and e=1. It applies for the following system.

Fig. 1.1

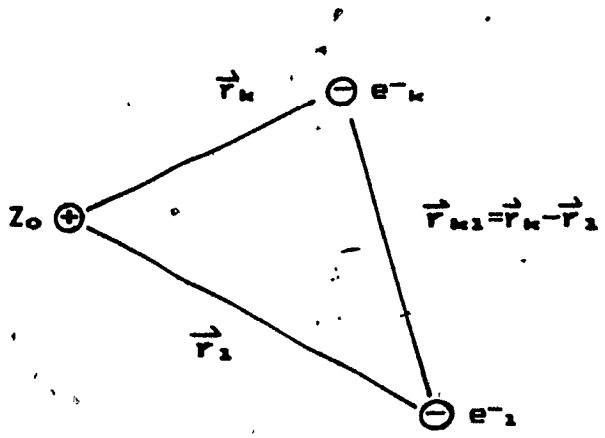

If the center of mass of the atom is at rest

$$\sum_k \vec{p}_k = 0 \quad . \tag{1.2}$$

The energy levels are given by the eigenvalues of (1.1), and so we get:

$$H_\infty \ \psi(r) = E_\infty \ \psi(r). \tag{1.3}$$

In the case of a finite nuclear mass the Hamiltonian is modified to allow for motion of the nucleus of mass M_A. If we now assume the center of mass of the atom to be at rest we have;

$$H_{MA} = \sum_k p_k^2/2m_e - \sum_k Z_o/r_k + \sum_{k<l} 1/r_{kl} + P_N^2/2M_A \ , \tag{1.4}$$

where P_N is the momentum of the nucleus. We also have;

$$\text{a)} \quad \vec{P}_N + \sum_k \vec{p}_k = 0$$

(1.5)

$$\text{b)} \quad P_N^2 = \sum_k p_k^2 + \sum_{k \neq l} \vec{p}_k \cdot \vec{p}_l \ .$$

From these we get:

$$H_{MA} = \sum_k p_k^2/2\mu + 1/2M_A \sum_{k \neq l} \vec{p}_k \cdot \vec{p}_l - \sum_k Z_o/r_k + \sum_{K<l} 1/r_{kl} \tag{1.6}$$

where $1/\mu = 1/m_e + 1/M_A$.

Hence the energy levels are now different and are given by;

(1.7) $$H_{MA}\,\psi_{MA}(r) = E_{MA}\,\psi_{MA}(r).$$

The following variable substitution will make the finite mass Hamiltonian contain a part that looks like the infinite mass equation, so the same wave function will solve both. The eigenvalues will be multiplied by a nuclear mass-dependent coefficient and a perturbation term will appear.

Do the variable substitutions:

(1.8) $\vec{r}_k' = \mu/m_e\,\vec{r}_k$ and $\vec{p}_k' = m_e/\mu\,\vec{p}_k$ (because $\vec{p}_k = -i\vec{\nabla}_k$).

This gives:

$$(1.9)\quad H_{MA} = \mu/m_e\left[\sum_k p_k'^2/2m_e - \sum_k Z_o/r_k' + \sum_{k<l} 1/r_{kl}' + \frac{1}{2(m_e+M_A)}\sum_{k\neq l}\vec{p}_k'\cdot\vec{p}_l'\right]$$

$$= \mu/m_e\left[H_\infty' + \frac{1}{(m_e+M_A)}\sum_{k<l}\vec{p}_k'\cdot\vec{p}_l'\right]$$

The eigenvalues of the first term are readily

found since the wave functions are known. Call this term H_{MA}^{∞}.

(1.10) From $H_{MA}^{\infty}=(\mu/m_e)\ H'_{\infty}$ we get $E_{MA}^{\infty}=(\mu/m_e)\ E_{\infty}$.

The normal mass shift is:

$$(1.11)\qquad \Delta E^{NMS}= E_{MA}^{\infty}-E_{\infty} = -\frac{m_e}{M_A}\ E_{MA}^{\infty}\ .$$

We may write $E_{MA}^{\infty}=E^{exp}{}_{MA}$, where $E^{exp}{}_{MA}$ is the experimentally measured energy of the level if the perturbation term of (1.9) is small. And so:

$$(1.12)\qquad \Delta E^{NMS}{}_{MA}= -\frac{m_e}{M_A}\ E^{exp}{}_{MA}\ .$$

The quantity which will eventually be measured is the frequency shift between two isotopes A' and A for the same transition "1". Now evaluate the contribution of the normal mass shift to the frequency shift. The transition is between a lower level E_1 and an upper level E_2 and is given by the following expression if the normal mass shift is taken into account:

$$(1.13)\ \delta\nu^{\wedge}{}_{1;NMS}=E_1-\frac{m_e}{M_A}\ E_1-E_2+\frac{m_e}{M_A}\ E_2.$$

$$=(E_1-E_2)-\frac{m_e}{M_A}\ (E_1+E_2)\ ,\ \text{with } h=1.$$

A similar expression is found for isotope A' and the difference in the transition frequency due to the normal

mass effect is given by:

$$(1.14)\quad \delta\nu^{AA'}{}_{1,NMS} = m_e (E_1-E_2)\,(M_{A'}-M_A)/(M_AM_{A'}) = M_{1,NMS}\, M_{AA'}\,, \quad M_{AA'}=(M_{A'}-M_A)/(M_AM_{A'})$$

where the convention is to take $\nu^{A'}-\nu^{A}$ for $M_{A'}$ greater than M_A.

In the same manner, we may evaluate an expression giving the frequency shift due to the perturbation term of the Hamiltonian (1.9). To first order, using the same wave function as before we get:

$$(1.15)\quad \Delta E^{NMS}_{MA} = \mu/m_e \left\langle \psi(r') \left| \frac{1}{2(m_e+M_A)} \sum_{K\neq L} \vec{p}_K' \cdot \vec{p}_L' \right| \psi(r') \right\rangle = 1/M_A \left\langle \psi(r) \left| \sum_{K<L} \vec{p}_K \cdot \vec{p}_L \right| \psi(r) \right\rangle$$

Again we look at a transition "i" between levels E_1 and E_2 for the two isotopes A' and A.

$$(1.16)\quad \delta\nu^{AA'}{}_{i,SMS} = (1/M_{A'}-1/M_A)\left[\left\langle \psi_1 \left| \sum_{K<L} \vec{p}_K \cdot \vec{p}_L \right| \psi_1 \right\rangle - \left\langle \psi_2 \left| \sum_{K<L} \vec{p}_K \cdot \vec{p}_L \right| \psi_2 \right\rangle \right]$$

$$= M_{AA'}\, M_{i,SMS}\,,$$

where $M_{AA'}$ is defined in (1.14) and $M_{i,SMS}$ contains the difference in the expectation values of $\sum_{K<L} \vec{p}_K \cdot \vec{p}_L$ between the upper and lower state, and is called the electron correlation term.

Thus the total frequency shift due to mass effects is

$$(1.17)\quad \delta\nu^{AA'}_{1,MS}=M_{AA'}\cdot(M_{1,NMS}+M_{1,SMS})\ ,$$

where the quantity in brackets is independent of the isotopes involved but depends only on the transition.

1.2.2) Field shift

The extended nuclear charge has a shifting effect only on transitions involving s electrons and transitions in which the screening of the inner closed s shell is changed. In the model used the nuclear charge is spherically symmetric and of radius R. The energy shift ΔE^{FS} is due to the difference in electrostatic potential between the extended charge, $V(r)$, and a point charge, $V_o(r)$. Thus;

$$(1.18)\quad \Delta E^{FS}=\int_0^\infty \psi^*[V(r)-V_o(r)]\psi\, 4\pi r^2\, dr\ ,$$

which is non-vanishing only inside the nuclear radius. The value of $\psi(r)$ may be taken constant inside the nucleus and equal to $\psi(0)$. The field shift is then given by:

$$(1.19)\quad \Delta E^{FS}=|\psi(0)|^2\int_0^R [V(r)-V_o(r)]\, 4\pi r^2\, dr\ .$$

For a uniform charge distribution, Gauss' law and the condition that $V(r=R)=V_o(r=R)$ gives;

(1.20) a) $V(r) = 3/2\ [\ 1/3\ (r/R)^2 - 1\ ]\ Ze^2/R\ ,\ r < R$

b) $V_o(r) = -Ze^2/r\ ,\ r \geq R\ .$

Put (1.20) into (1.19) to find;

(1.21) $\Delta E^{FS} = |\psi(0)|^2\ 4\pi/10\ e^2 Z \cdot R^2\ .$

For two isotopes A and A' it is assumed that the energy difference is due only to a difference in nuclear radius. Thus for the level E_1 the shift is:

(1.22) $-\delta(\Delta E^{FS}_1)_{AA'} = |\psi(0)|^2_1\ 4\pi/10\ e^2 Z\ \delta R^2$

and a similar expression is found for the level E_2. The field shift in the transition "i" between isotopes A and A', whose charge radii are different δR is:

(1.23) $\delta\nu^{AA'}_{i,FS} = \delta(\Delta E^{FS}_1) - \delta(\Delta E^{FS}_2)$

$= 4\pi/10\ e^2\ Z\ \delta R^2\ [\,|\psi(0)|^2_1 - |\psi(0)|^2_2\,]\ .$

Generally the literature writes about the mean square charge radius, $\delta\langle r^2\rangle = 3/5\ \ \delta R^2$. Finally, the field shift is:

(1.24) $\delta\nu^{AA'}_{i,FS} = F_i \, \delta^{AA'}\langle r^2 \rangle$.

As in the cases of NMS and SMS, the frequency shift is expressible in terms of a strictly isotope dependant term, $\delta\langle r^2 \rangle$ and an electronic term F_i.

1.2.3) King plots

The total isotopic shift for the transition labelled "i", between isotopes A and A' is the sum of the three effects just described;

(1.25) $\delta\nu^{AA'}_i = \delta\nu^{AA'}_{i,NMS} + \delta\nu^{AA'}_{i,SMS} + \delta\nu^{AA'}_{i,FS}$

$= M_{AA'} \, M_{i,NMS} + M_{AA'} \, M_{i,SMS} + F_i \delta\langle r^2 \rangle$.

One wishes to extract from isotope shift measurements the change in mean square distribution of the nuclear charge when pairs of neutrons are added. First the normal mass shift part of the total shift is calculated easily, from equation (1.14), and subtracted from the measured value. Remaining is the sum of the FS and SMS which are not easily separated.

(1.26) $\delta\nu^{AA'}_{i,FS+SMS} = M_{AA'} \, M_{i,SMS} + F_i \delta\langle r^2 \rangle$.

$M_{i,SMS}$ contains the electron correlation term

which is not calculable. F_i involves the calculation of the change in electronic density at the nucleus during the transition. This electronic factor has been calculated for the 557 nm transition (5s[3/2]2-5p'[1/2]1) in Kr [Ger 79] and also a model dependent value for $\delta^{84-86}\langle r^2\rangle$ has been found. From these two values it is possible to evaluate, first, the F_i for any Kr transition for which the shifts are known for at least three isotopes, and second, the $\delta\langle r^2\rangle$ for any pairs of these isotopes. Thus, if shifts were measured on the same isotopes for another transition "j", the "i" and "j" equations giving the sum of the FS and the SMS may be combined to give;

$$(1.27)\quad \delta\nu^{AA'}_{i,FS+SMS}/M_{AA'} = F_i/F_j\,[\delta\nu^{AA'}_{j,FS+SMS}/M_{AA'}] + [M_{i,SMS} - F_i/F_j\, M_{j,SMS}] \ .$$

Plotting $\delta\nu^{AA'}_{i,FS+SMS}/M_{AA'}$ as a function of $\delta\nu^{AA'}_{j,FS+SMS}/M_{AA'}$ for at least two measured shifts will give a line whose slope is F_i/F_j and the offset is $M_{i,SMS}-F_i/F_j\, M_{j,SMS}$. This is called a King plot [Kin 84b]. In the case of krypton, F(557 nm) and $\delta^{84-86}\langle r^2\rangle$ are known. Thus F(587 nm) is known from the slope of (1.27) and the SMS will be separable from the FS and $\delta^{AA'}\langle r^2\rangle$ will be calculable for any Kr isotope pair. It must be remembered that any evaluation of the SMS or of $\delta^{AA'}\langle r^2\rangle$ ultimately relies on preliminary theoretical estimates.

CHAPTER 2: Laser Spectroscopy

This chapter will present briefly the most popular C.W. laser spectroscopic techniques, starting with Doppler-limited and then Doppler-free techniques. The second and most important part of this chapter deals in greater detail with Doppler-free polarisation spectroscopy, which is the technique used in the present work.

2.1) C.W. Laser spectroscopic techniques

2.1.1) Doppler-limited techniques

The first Doppler-limited technique to be discussed is absorption spectroscopy; a schematic of the necessary set-up is shown on fig. 2.1.

Fig. 2.1

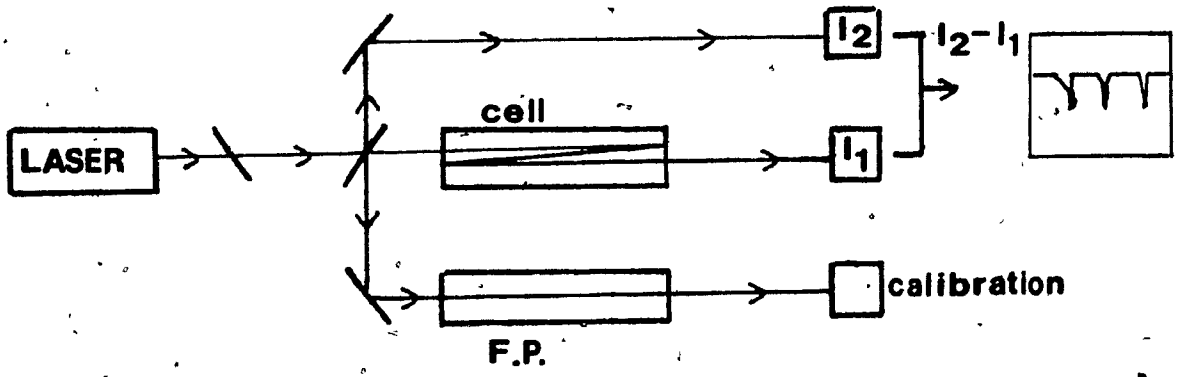

Absorption spectroscopy involves measuring the transmitted intensity of a frequency tunable laser beam making multiple passes inside a cell containing a mixture of isotopes in gaseous form. As the laser frequency is scanned in a linear fashion, the beam will encounter a varying absorption coefficient around the real or Doppler-shifted transition frequencies of the atoms. The amount of absorbed intensity depends on the population, $N(\omega)$, i.e. the number of atoms whose transition frequency ω_o is Doppler-shifted to ω, the frequency of the laser. $N(\omega)$ is a Gaussian function which peaks at ω_o. The absorption cross-section of each atom follows a resonance profile whose width depends only on the linewidth of the transition. Hence, the final absorption profile is a convolution of the Gaussian and the Lorentzian functions and is given by;

$$(2.1) \qquad I(\omega) = C' \int_0^{\infty} \frac{\exp[-(c(\omega_o-\omega')/\omega_o v_p)^2]}{(\omega-\omega')^2+(\gamma/2)^2}\, d\omega'$$

which is called a Voigt profile [Dem 81a].

On fig. 2.1 the absorption profile is given by I_1-I_2 and is calibrated in frequency using a Fabry-Perot etalon of fixed mirror separation whose mode spacing is accurately known. The reference signal I_2 is used to cancel fluctuations in the laser output intensity.

The mirror image of an absorption spectrum is an excitation spectrum. In its simplest form, excitation spectroscopy just involves the detection and counting of

individual fluorescent photons. The integration of the number of counts over short time intervals compared to the scan time is translated into an intensity profile $I(\omega)$. The setup is essentially the same as the one depicted on fig. 2.1 except that the P.M. is aimed at the gas cell. In order for this technique to be applicable, certain conditions must be met; the probability of deexcitation through non-radiative processes must be low, the lifetime of the excited state must be much smaller than the count integration time (i.e. the excited atom must not drift out of the solid angle of the photodetector) and the detector must have a constant quantum efficiency over a wide part of the spectral range.

In the techniques described above, the signals involved are usually very small. The background noise may be reduced by chopping the laser beam (modulating the amplitude) or modulating the laser frequency. The detected signal will be at a frequency corresponding to the modulation and may be discriminately amplified by a lock-in amplifier. More will be said later on the frequency modulation method since it is the one used in the present work.

Still another technique is that of optogalvanic spectroscopy. It involves the measurement of the change in effective resistance inside a gas discharge which is optically pumped with a laser beam. A setup for this technique is shown on fig. 2.2

Fig. 2.2

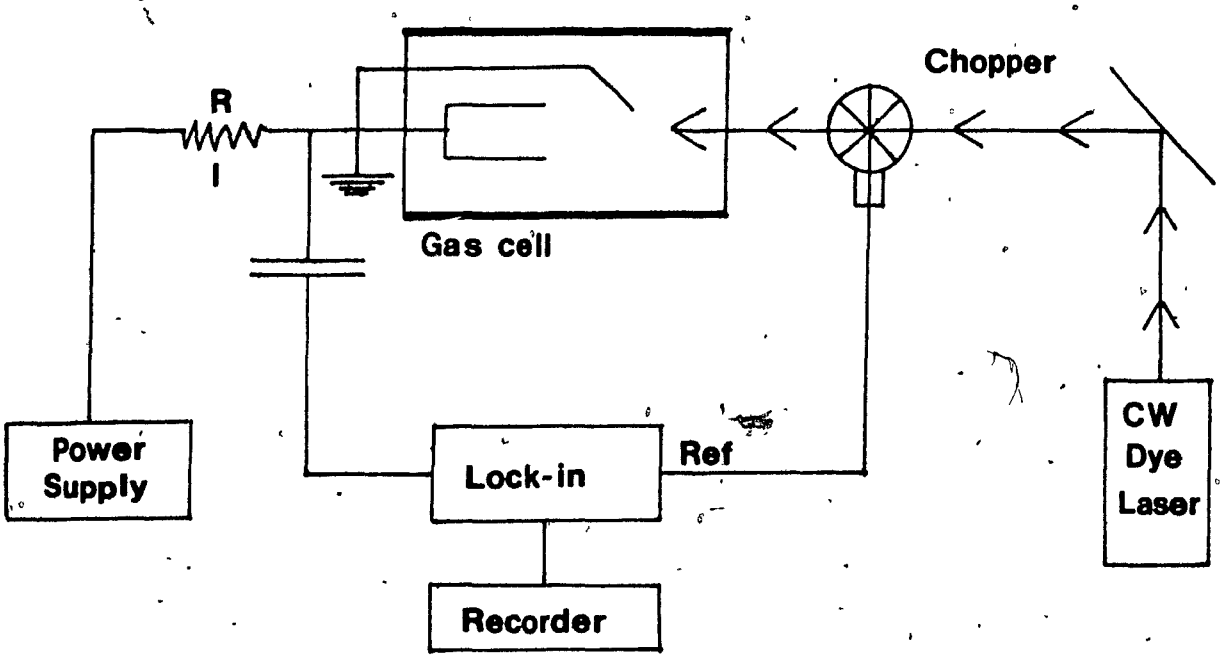

The laser pumps a lower level to an upper level, hence modifying their respective populations. Because of differences in ionization probability of these two levels, there results a change in the discharge resistance giving a change in the current at R. If the laser beam is chopped an a.c. voltage will be measured at R which can be fed directly into a lock-in amplifier. The voltage amplitude as a function of the laser frequency gives a spectrum.

If the upper level of the transition is close to the ionization limit, the technique of ionization spectroscopy may be used. The excited state may then be ionized through several processes. One of these is photoionization, and the whole technique is sometimes referred to as "two-photon ionization spectroscopy". Fig.

2.3 shows a set-up used in this technique and the energy level diagram.

Fig. 2.3

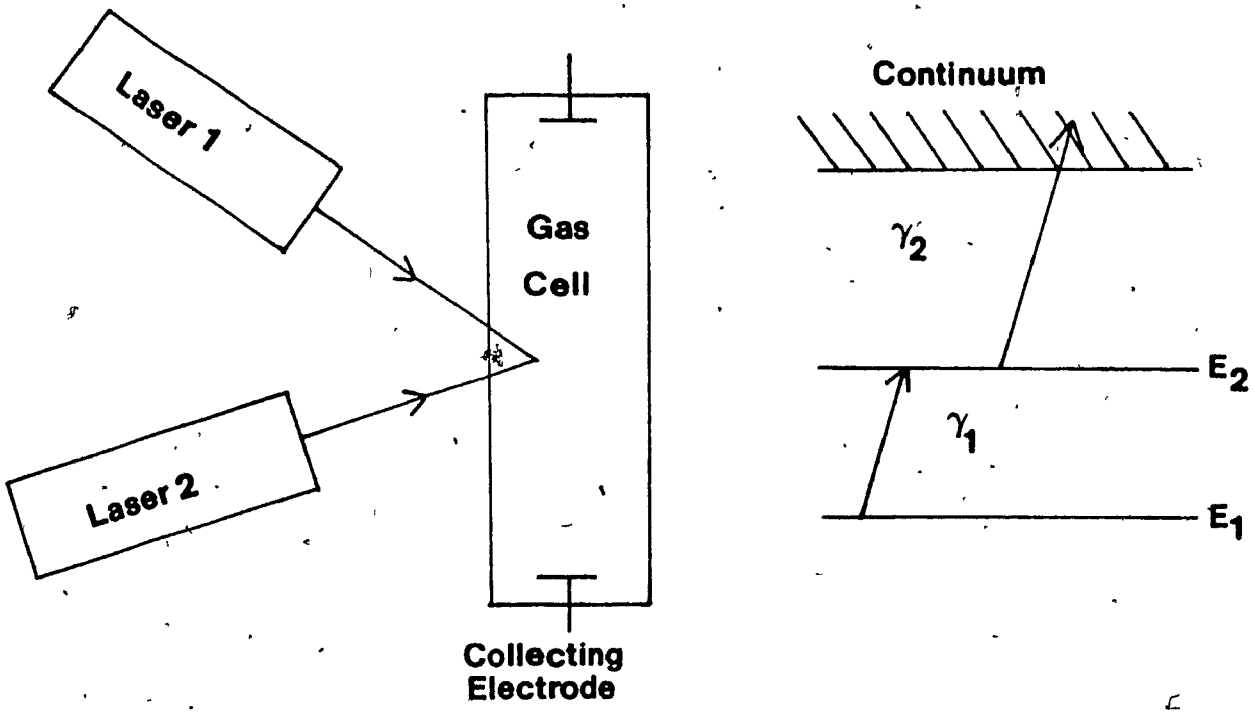

Only the beam pumping to the lower level need be tunable, the other may be of fixed frequency but must be of sufficient energy to bring the excited electron over the ionization limit.

In other schemes the excited atom may be ionized through collision with a buffer gas or through the application of a strong electric field. In all the methods just described, the signal is made up of the collected electrons.

This concludes the overview of the Doppler-limited techniques although other more exotic techniques exist [Dem 81b].

2.1.2) Doppler-free techniques

The techniques just described are of little use for doing isotopic shifts measurements on Kr, which are all around 100 MHz, because this is the order of the Doppler broadening at room temperature. Doppler-free methods must be used. They involve the sampling and measurement of a transition on subgroups of atoms which have a very small velocity component along the direction of the laser beam. Many of these techniques are refinements of the Doppler-limited ones; they will be described in the present section.

Let us first examine the technique of laser spectroscopy on an atomic beam. As stated before it was used by Champeau [Cha 78] on Kr in 1978. This techniques may be either of the absorption or excitation types. Fig. 2.4 shows a possible setup.

Fig 2.4

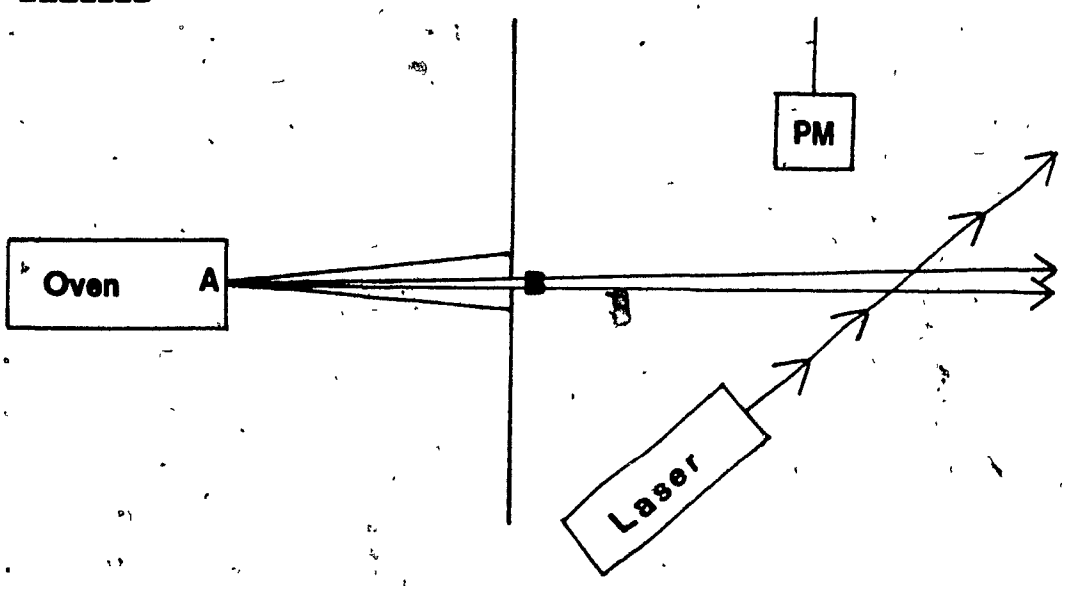

Atoms to be studied are initially collected and put in an oven. The oven is heated and the atoms boil off to form a narrow beam collimated through a slit. The probing laser beam is incident at a right angle to the atomic beam. Thus only the very small transverse component of an atom's velocity contributes to Doppler broadening of the transition. This technique offers the very interesting possibility of spectroscopic measurements on short lived mass-separated isotopes, since very rapid on-line collection and reemission of these isotopes is possible.

Doppler-free spectroscopy may also be done on atoms contained in a cell. One such method is a modification on the absorption technique just described and is called saturation spectroscopy. At any laser frequency, the amount of absorbed intensity is determined by the population of atoms available in the absorbing lower state. In saturation spectroscopy a strong saturating pump beam depletes the lower level, thus effectively decreasing the absorption coefficient for a weaker probe beam going through the same volume of gas. For this effect to occur, the two beams must interact with the same group of atoms. If the beams are made to go in opposite directions they simultaneously interact only with atoms at rest along the beam axis, i.e. at the natural line of the transition. The laser linewidth becomes the limiting factor on the resolution. Fig. 2.5 shows a rough schematic of a saturation spectroscopy setup.

Fig 2.5

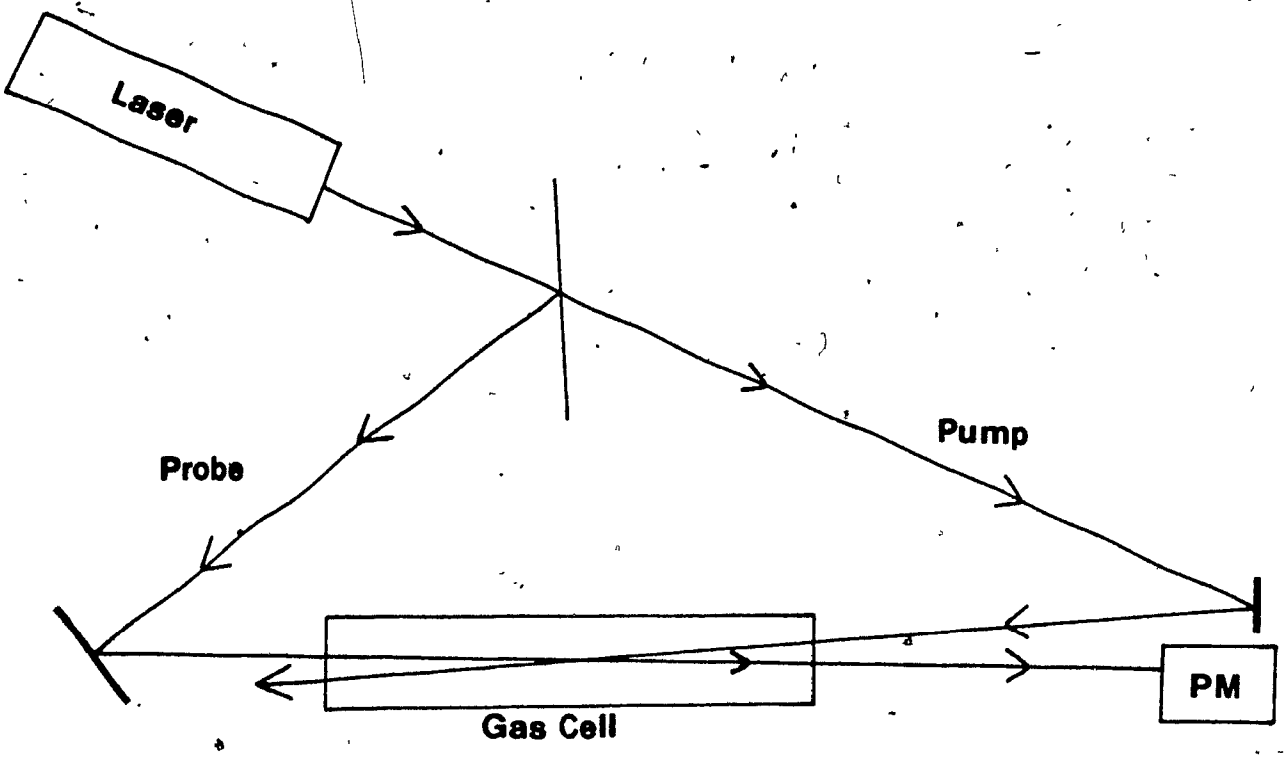

A saturation spectrum displays peaks corresponding to a maximum transmission of the probe beam at the transition frequency.

The next section deals with the polarisation spectroscopy technique used in the present work. Other techniques are described in the literature [Dem 81c].

2.2) Polarisation spectroscopy

2.2.1) The technique.

In the case of Kr the isotopic shift is masked by the Doppler broadening of the transition. Say v_z is the velocity component along the laser beam axis of a certain subgroup of atoms. The natural frequency of the transition is Doppler-shifted with respect to the laser beam according to;

(2.1) $$\omega=\omega_o+\vec{k}\cdot\vec{v} .$$

In fact, due to the finite line-width of the laser, $\delta\omega$, interaction of the beam will occur with atoms whose velocities are within an interval Δv_z of v_z so that;

(2.2) $$\omega+/-\delta\omega=\omega_o+k\cdot v_z+/-k\cdot\Delta v_z .$$

Doppler-free polarisation spectroscopy relies on the anisotropic orientation of the absorbing atoms' angular momentum vector and on the birefringence that is produced in an atomic vapor by an intense polarised saturating pump beam. This will cause a linearly polarised probe beam, that interacts with the same subgroup of atoms, to become

elliptically polarised with its major axis tilted with respect to the original polarisation. The technique is Doppler-free if the two beams go in opposite directions for the same reasons as in the case of saturation spectroscopy. Fig. 2.6 show a schematic of the experimental setup needed for polarisation spectroscopy.

Fig. 2.6

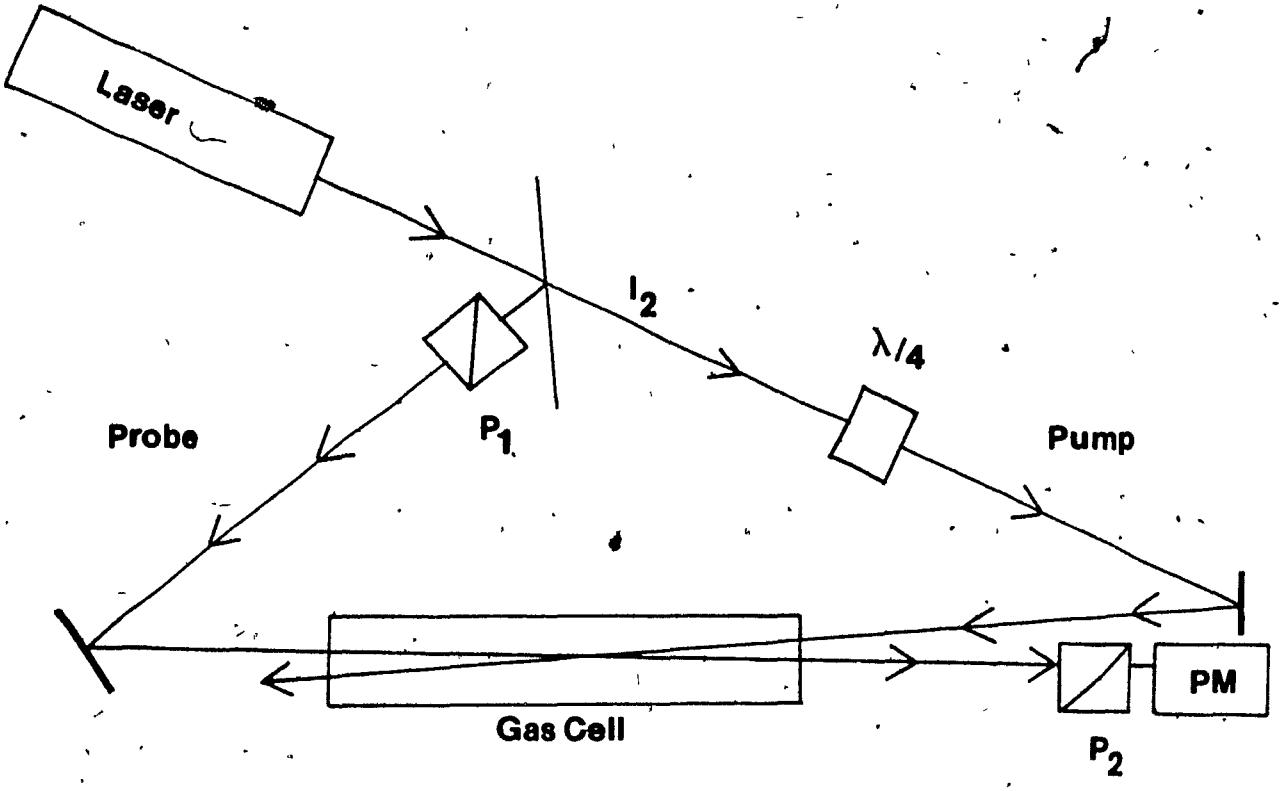

The linearly polarised beam I_2 is circularly polarised as it goes through a quarter-wave plate. As the laser frequency is tuned to the atomic transition (J",M)-(J',M+/-1), absorption of the pump beam occurs. Selection rules require that M=+/-1 for left and right hand polarisation, where M is defined along the z axis parallel to the beam direction. The result will be a non-isotropic

angular momentum distribution of the population of atoms in the initial state J" and/or the final state J', depending on the value of ΔJ, as shown by fig. 2.7.

Fig. 2.7

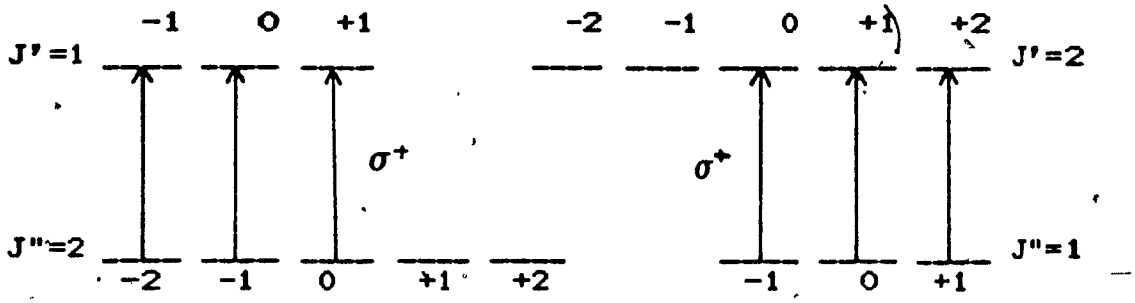

The counter propagating linearly polarised probe beam may be seen as the sum of a right and left hand circularly polarised wave (σ^+ and σ^-). Due to the saturation effect of the pump beam, the available populations of absorbing atoms are different for the σ^+ and σ^- components of the probe. This amounts to having different absorption coefficients α^+ and α^-, and different optical paths (giving two indices of refraction n^+ and n^-) for the two components. Summing of the remaining waves after a path length L in the saturated gas leaves a net elliptical polarisation with the major axis tilted with respect to the original polarisation direction.

A polarisation spectrum thus involves measuring the light intensity of the probe beam transmitted through a polariser, whose axis is almost perpendicular to the

original probe polarisation, as the laser frequency is varied.

2.2.2) The polarisation spectrum

In this section the equation of a polarisatiion spectrum will be derived. Call z the axis parallel to the beam and x and y the two perpendicular directions. The linearly polarised probe beam may be written as;

(2.3) $E = E_o e^{i(\omega t - kz)}$, with $E_o = (E_{ox},0,0) = (E_o,0,0)$.

We may treat E as the sum of a right and a left circularly polarised wave by putting:

(2.4) $E_o = E_o/2 + iE_o/2 + E_o/2 - iE_o/2$,

all amplitudes being equal because of circular polarisation.

Since each component has in the saturated gas different α and k, with $k=\omega n/c$, we find that after a path L through the gas:

(2.5) $E^+ = E_o/2\ (1+i)\ e^{i(\omega t - k^+ L + i\langle \alpha^+_z \rangle L)}$

$E^- = E_o/2\ (1-i)\ e^{i(\omega t - k^- L + i\langle \alpha^-_z \rangle L)}$

At z=L the total probe wave is $E=E^{+}+E^{-}$. The crossed polariser is along the y direction. Of relevance is the y component of the final wave:

$$(2.6)\quad E_y = iE_o/2\ (e^{i(\omega t-k^{+}L+i(\alpha^{+}/2)L)}-e^{i(\omega t-k^{-}L+i(\alpha^{-}/2)L)})$$

$$= -iE_o'/2\ (e^{i(k^{+}-k^{-}-i(\alpha^{+}-\alpha^{-})/2)L+i2b}-1)\ e^{i(\omega t+\varphi)}\ ,$$

where $\varphi=-k^{+}\cdot L$ and $E_o'=E_o\ e^{-\alpha/2\ L}$. The term 'b' in the exponent has been introduced to account for birefringence of the cell windows.

Usually $\Delta k=k^{+}-k^{-}$ and $\Delta\alpha=\alpha^{+}-\alpha^{-}$ are small and the exponent may be expanded to first order to get:

$$(2.7)\quad E_y = -E_o'\ (\theta+b+(\omega L/2c)(n^{+}-n^{-})-i(\alpha^{+}-\alpha^{-})L/4)\ e^{i(\omega t-\varphi)}\ ,$$

which is the transmitted amplitude through the crossed polariser. A constant term $E_o'\theta$ has been introduced to account for the transmitted amplitude if the polariser is at a small angle from the perfect crossing.

The differences $\Delta n=n^{+}-n^{-}$ and $\Delta\alpha=\alpha^{+}-\alpha^{-}$ depend on the laser and atomic transition frequencies. Taking the absorbing atom as a damped harmonic oscillator, we get a Lorentzian profile for [Dem 81d]. Thus:

(2.8) $\Delta\alpha = \alpha_o/(1+x^2)$, with $x=(\omega_o-\omega)/\gamma$, where γ is

the transition linewidth.

The frequency dependent absorption coefficient and index of refraction are related by the Kramers-Kronig dispersion relations [Dem 81e]. Thus

(2.9) $$\Delta n = \Delta\alpha_o \, c/\omega_o \, x/(1+x^2) \, .$$

The transmitted intensity is $I=E_y E_y^*$. From (2.7) through (2.9) we find

(2.10) $$I_t = I_o \, (\xi+\theta^2+b^2+(b/2\Delta\alpha_oL-1/2\Delta\alpha_oL) \, x/(1+x^2) + 1/4 \, (\Delta\alpha_oL)^2 \, 1/(1+x^2)) \, ,$$

where ξ has been introduced to account for a small residual transmission through the crossed polarisers. Equation (2.10) thus becomes:

(2.11) $$I_t = I_o \, (A \, x/(1+x^2)+B/(1+x^2)+C) \, ,$$

where the set of parameters A, B, w and γ characterises a peak on the polarisation spectrum, and C is a constant (usually externally added) offset.

The intensity of the signal I_t depends explicitly on α, the difference between the absorption coefficient of left and right hand circularly polarised waves. In terms of the cross-sections we may write:

(2.12) $$\Delta\alpha = \alpha^{+} - \alpha^{-} = n_M (\sigma^{+}_{J''J'M} - \sigma^{-}_{J''J'M}) ,$$

where $\sigma^{+/-}_{J''J'M}$ refers to the transitions J"M → J'M+1 and n_M is the volume density of the atoms in the sublevel M of the lower level J". The dependence of the σ's on M may be factored out explicitly using the Wigner-Eckart theorem giving:

(2.13) $$\sigma^{+/-}_{J''J'M} = |\langle J''M\ 1+/-1 |\ J''M+/-1\rangle|^2 \quad \sigma_{J''J'} .$$

Thus the magnitude of the polarisation signal will depend on the particular lower and upper level and this dependence shows up as a summation of Clebch-Gordon coefficients. Values for $\Delta\alpha$ in terms of the C-G coefficients have been tabulated explicitly [Tee 77] for J=0,+/-1 for linearly and circularly polarised pump beams. It turns out that for J=+/-1 it is advantageous to use a circularly polarised pump; this is what has been used in the present work.

2.2.3) Frequency modulation.

In the previous section it was found that the intensity spectrum as a function of the laser frequency is given by (2.11). Hence, determination of the isotopic shift

between isotopes A and A' for a transition "i" involves findinng the parameters of the equation describing the intensity spectrum; one of them being ω^{A}_{i}, the transition frequency. In fact, the absolute frequency is not found on a spectrum done over a limited frequency range, but differences in frequencies are given. Thus the IS is:

$$\delta\omega^{AA'}_{i} = (\omega^{A'}_{i} - \omega^{A}_{i}) \quad . \tag{2.14}$$

In a practical sense the polarisation signal to be detected is extremely weak and may not be detectable over the background. In the present work this problem is solved by modulating the laser frequency. This method was suggested by Pinard [Pin 86]. The polarisation signal will appear at the modulating frequency and may be discriminately amplified using a lock-in amplifier.

As the laser frequency "ω" is scanned it also has a small frequency modulation $\Delta\omega/2$. Thus the polarisation spectrum $I_e(\omega)$ is sampled in small intervals of width $\Delta\omega$ and the lock-in amplifier receives a peak to peak signal of $I_e(\omega + \Delta\omega/2)$ to $I_e(\omega - \Delta\omega/2)$. The spectrum will then have the shape of the derivative of the intensity, i.e., $I_e/\Delta\omega$, and is given by:

$$dI_e/d\omega = I_o' \left((A(1-x^2)-2Bx)/(1+x^2) + C' \right) , \tag{2.15}$$

where C' is an externally added offset, to keep the spectrum

positive, and I_o' regroups all the multiplicative constants. In the case of $I_\perp$, the appearance of resonance shaped peaks is favored by the selection of a small crossing angle of the polarisers (i.e., smaller than 1°) [Aud 85]. For the $dI_\perp/d\omega$ spectrum the opposite is true. For all the spectra shown in this work the crossing angles are around 2°.

Chapter 3: Experiment and Data

3.1) Experimental set-up and technique.

The following is a description of the experimental setup and technique, some elements of which will now be familiar to the reader from the previous section on polarisation spectroscopy. This section is divided into four parts: i) the vacuum and RF discharge systems, ii) the laser and optical components, iii) the signal, processing and data acquisition system, and finally, iv) a short section on the signal optimisation.

3.1.1) The vacuum and RF discharge systems

Figure 3.1 shows a schematic of the vacuum system. As is typical of such systems a roughing line, which uses a mechanical pump, brings the pressure down to the operating range of a turbo-molecular pump. The capacitance gauge operates in the mTorr range; it was checked with a McLeod mercury gauge and found to be correct to within +/- 5 mTorr. Two gas inlet valves make possible varied mixtures of natural Kr and enriched isotopes (stable and eventually radioactive). It has been shown [Aud 85] that Kr pressures of 50 to 100 mTorr give the best polarisation signals.

FIGURE 3.1 VACUUM SYSTEM

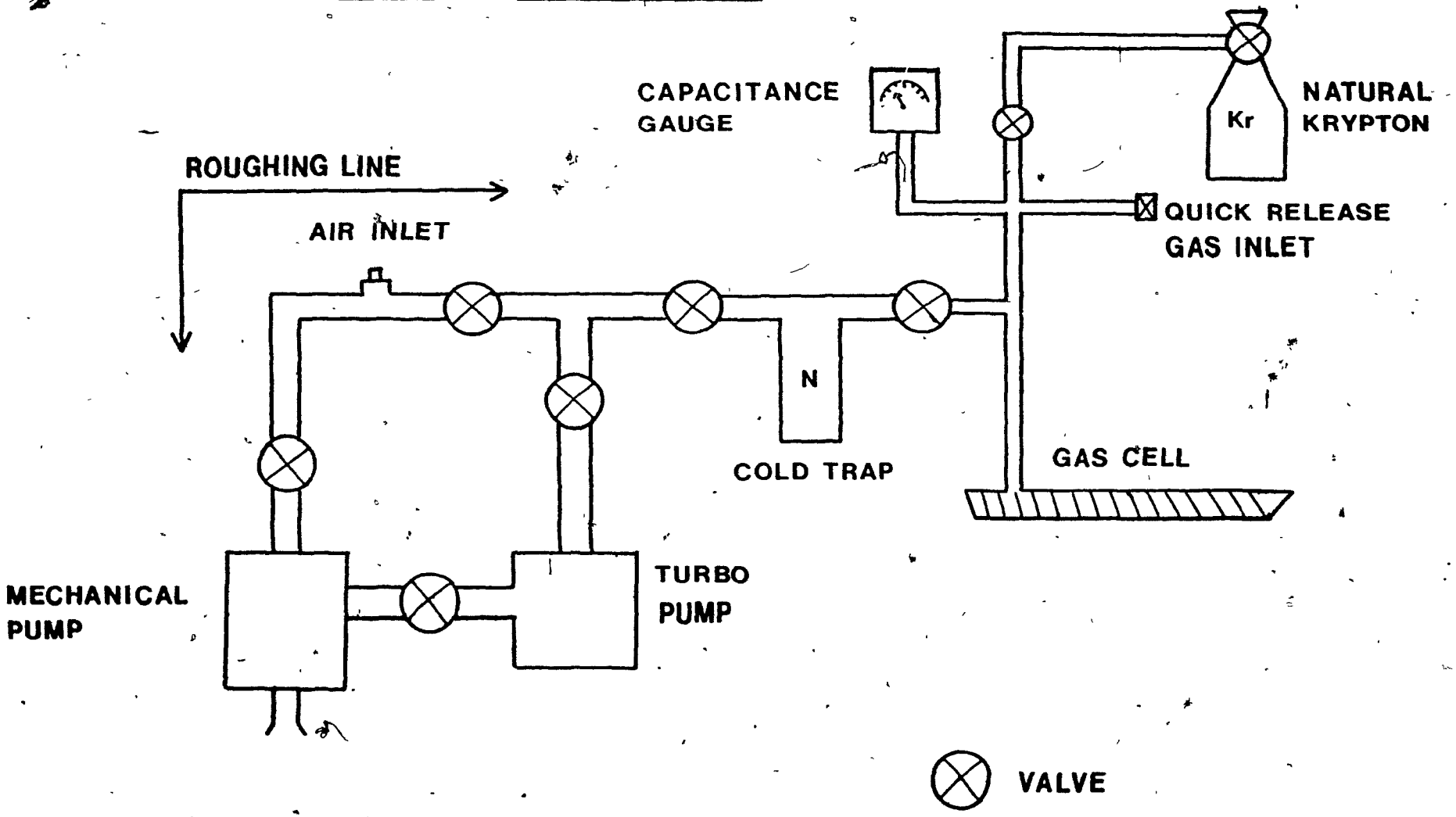

The first excited state of Kr lies 10 eV above the ground state. For this reason the lower levels of optical transitions must be excited states. The lower level of the 587 nm transition is the short lived 5s[3/2]1. The Kr gas cell is wound with a primary coil which carries an RF signal. The secondary circuit is an LC circuit with the secondary coil also wound around the gas cell. The Kr gas is excited via the RF discharge when the input signal is at the resonance of the LC circuit. Again it was shown by Audet [Aud 85] that the best polarisation signals are obtained for transmitted powers of 5 to 20 watts. The RF signal frequency is digitally varied around 30 MHz until the best discharge and power transmission are obtained.

3.1.2) The optics

The schematic of the laser system, spectrum analysing instruments and related optics are depicted in figure 3.2. A C.W. ring dye laser is used to get a tunable beam of monochromatic photons. The dye used is Rhodamine 6G which has a wavelength range of 560 to 610 nm with a peak at roughly 580 nm. At 587 nm it is possible to get 300 to 400 mW of continuous power. The dye laser is pumped with a 6 W beam of 514 nm photons from an argon ion gas laser.

The signal processing technique described in chapter 2 calls for the frequency modulation of the dye

laser. The laser is equipped with a frequency stabilizing feedback circuit which measures any drift in frequency and sends a correcting signal to one of the laser cavity mirrors mounted on a piezoelectric crystal. This system reduces the jitter to 1 MHz. The frequency is modulated by driving the crystal with a 1.5 KHz sine wave voltage of small amplitude. Fine tuning of the signal frequency and amplitude is done at the time of the experiment to optimize the polarisation signal.

A rough estimate of the laser wavelength is obtained from a wavemeter. The stability of the laser is monitored using a spectral analysing etalon which has mode spacings of 151.3 +/- 0.8 MHz. During the experiments, an etalon spectrum is recorded for fixed mirror spacing and this serves as a frequency calibration for the associated IS spectrum. The laser frequency is scanned over 5 GHz so that the outer Kr^{83} hyperfine structure peaks may be observed.

The dye laser beam is linearly polarised at P_1. The thick glass plate SR3 is used as a beam splitter; it gives two reflections, one on its front and the other on its back face. This double probe beam is sent along the axis of the gas cell. The left probe beam on fig. 3.2 is the signal beam which is overlaping with the pump beam. The other probe beam gives a reference signal at PM_{ref} which is used in part to cancel birefringence of the cell windows or the finite extinction of the crossed polarisers, P_1 and P_2. However, its main function is the cancellation of the Doppler

broadened absorption spectrum. More will be said on this later.

The transmitted beam at SR3 carries about 90% of the original intensity. It becomes circularly polarised at the $\lambda/4$ plate. It then reflects on M4 and counter propagates inside the gas cell with a maximum volume overlap with the signal probe beam.

3.1.3) Signal processing and data acquisition systems.

Figure 3.3 shows the signal processing and data analysis circuitry. For clarity, some of the optical components are reproduced here.

The relative sizes of the PM_{sig} and PM_{ref} signals are varied before subtraction. This is done with a differential amplifier (DOP) which was built by Audet [Aud 85]. The resulting signal is amplified with a lock-in amplifier whose reference is at the same frequency as the frequency modulation of the laser. This eliminates the need for an external beam chopper and completely cuts out any background light. This way one obtains the derivative of the polarisation spectrum as described in chapter 2.

The etalon and polarisation spectra are recorded simultaneously. A digital-to-analog converter (DAC) supplies the external ramp voltage to the appropriate component inside the laser cavity for frequency scanning. The size and

duration of this ramp voltage is determined by the experimenter as the selections of scan time and width are made.

The data acquisition system and scan triggering and control are done from a computer which communicates with the analog-to-digital converters (ADC) and the DAC through a CAMAC interface.

3.1.4) Optimization of the signal

Some additional precautions are taken in order to optimize the signal.

The RF driven coils around the cell emit microwave radiation which may contribute to background noise in the electronics, and disturb the scanning of the laser. The problem is solved by enclosing the cell and coils inside a fine wire mesh cage that acts as a Faraday cage. As well, the windows of the cell are slightly angled to prevent reflections of the pump beam back into the detectors; because of its circular polarisation and intensity it would not be completly cut at P_2 and would saturate the detectors.

Final signal optimisation is achieved through the proper balancing of the reference and signal probe beams, proper phase adjustement of the lock-in amplifier and maximum overlap of the probe and pump beam.

Fig. 3.2 Optics

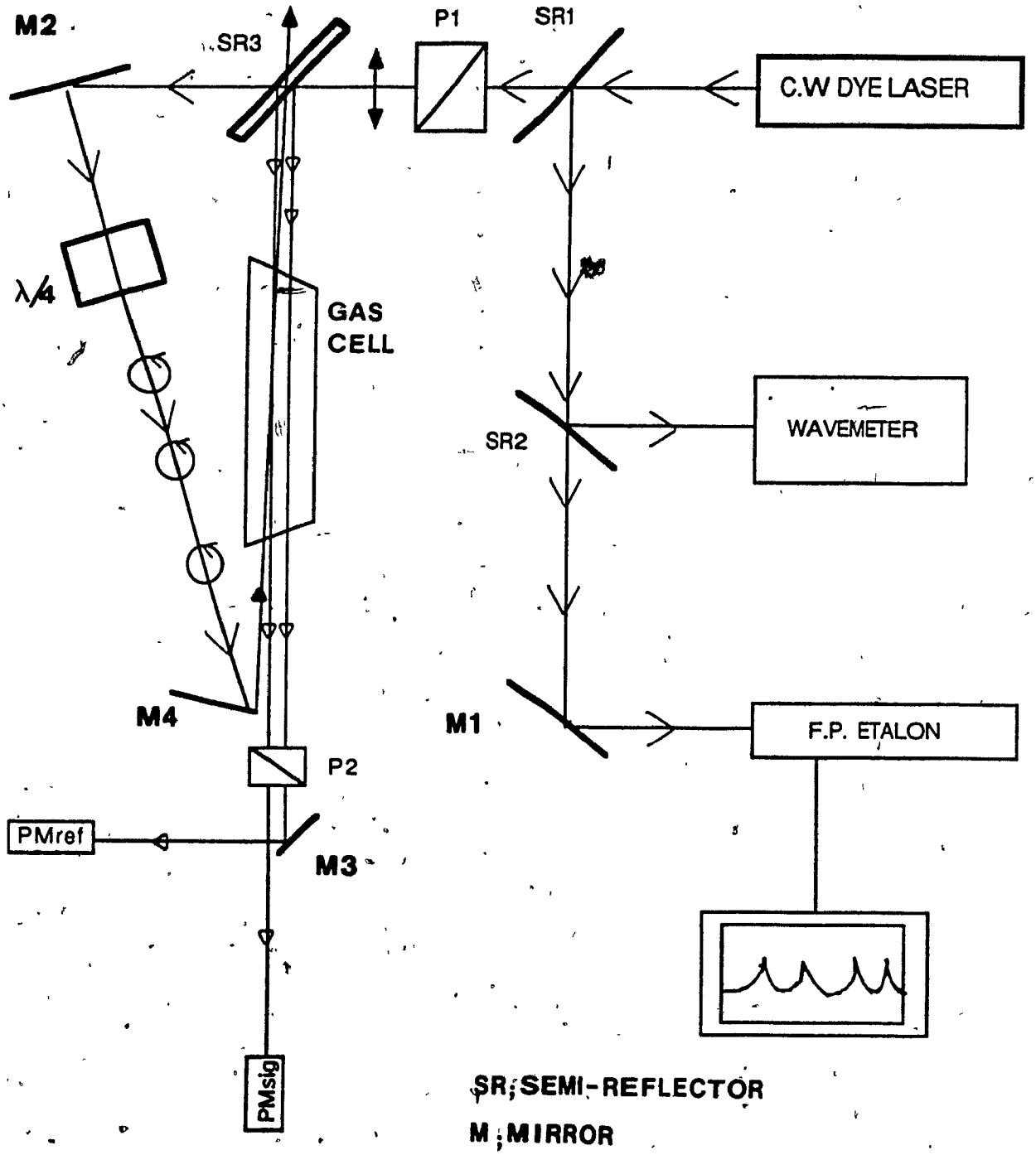

FIGURE 3.3 ELECTRONICS AND DATA ACQUISITION SYSTEM

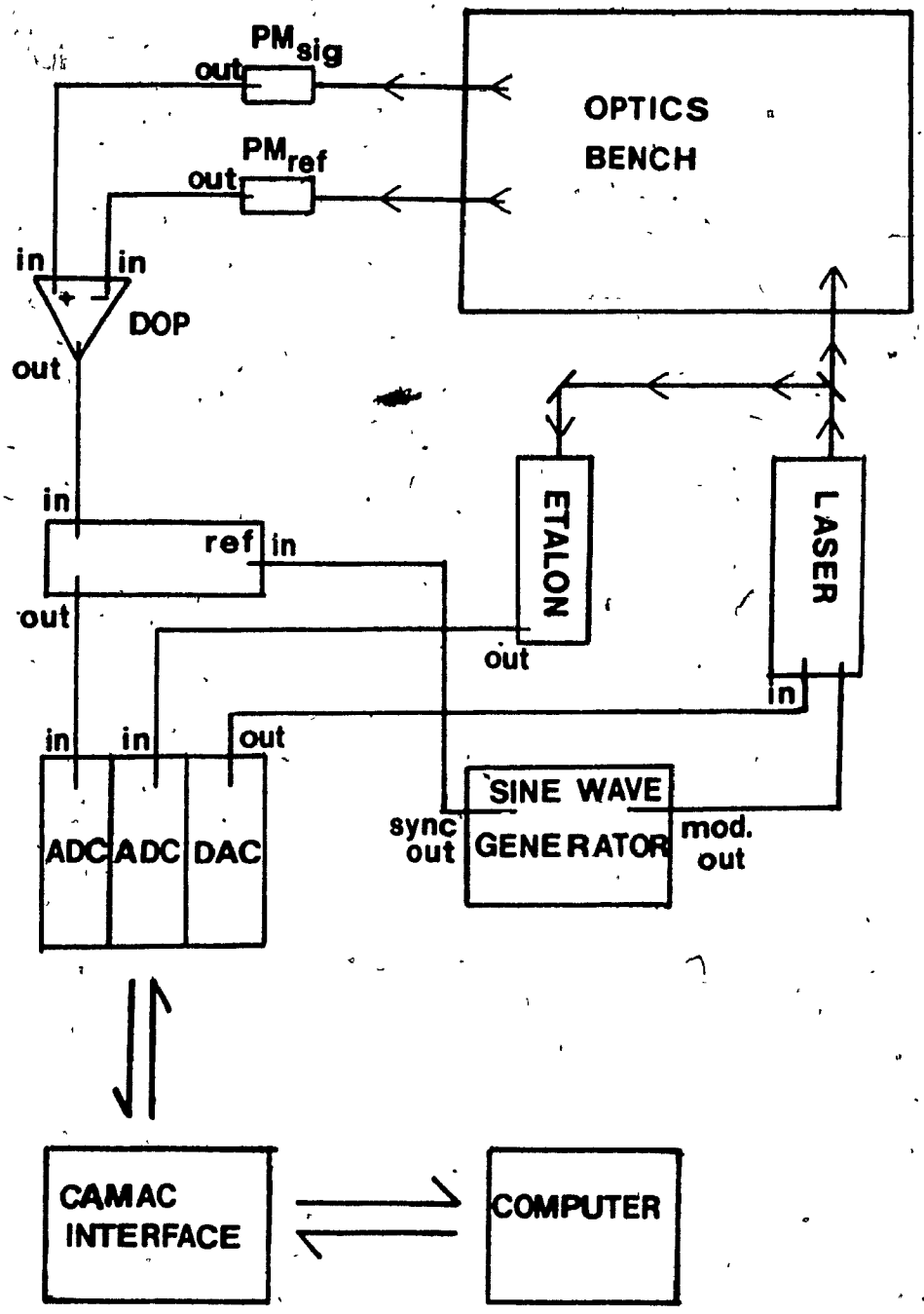

3.1.5) Data processing.

In order to calibrate the frequency axis of the IS spectrum one records simultaneously an etalon spectrum. This consists of the light intensity on the output side of a F.P. etalon of fixed mirror spacing giving the familiar Airy function (see fig. 3.4b). The spectrum calibration is determined using a specially written program which finds the centroid of each peak and averages multiple peaks (which are due to slight laser instability and the frequency modulation). The average interpeak distance is found and the spectrum is calibrated using the known mode spacing.

Etalon peaks are also used by the data acquisition program to trigger scans when multiple scans and summing are desired. This, in principle, ensures perfect channel to channel correspondence between scans. This option could not be used in this work because of the frequency modulation; it gave wider etalon peaks of imperfect shape leading to an uneven trigger from scan to scan. The spectrum shown in this work are made up of single scans which were summed after the experiment with proper horizontal offseting. Typically, each spectrum consists of the summation of 4 or 6 scans, but in one case 16 individual scans were added.

3.2) Spectrum.

Isotopic shift measurements have been done repeatedly on Kr isotopes in natural abundance and on mixtures containing enriched amounts of Kr^{78}. Some of the resulting spectra will be shown in the following section. Reference may be made to appendix A for the description of the Kr spectra.

3.2.1) Natural Kr.

Natural Kr consists of five even and one odd isotopes in the following abundances [Ger 77]; Kr^{78} (0.35 %), Kr^{80} (2.27 %), Kr^{82} (11.56 %), , Kr^{83} (11.55 %), Kr^{84} (56.90 %) and Kr^{86} (17.37 %). The transition studied is 5s[3/2]J=1 to 5p'[3/2]J=2.

Figure 3.4 a) shows a spectrum of 5.6 GHz width of natural Kr and 3.4 b) shows the related etalon spectrum. The various peaks may be identified on the basis of their relative intensities. One may also rely on the fact that the main contribution to the total shift comes from the normal mass shift and is given by:

(3.1) $\delta\nu^{AA'}_{i,NM} = M_{AA'} M_{i,NM}$,

and is positive for M_A greater than M_A.

In the case of the hyperfine structure peaks, matters are a little more complicated. The total angular momentum J couples with the nuclear spin I to give F=J+I, where F may take any value from J+I to J-I in unit steps. The energy of a state defined by a particular J, I and F is displaced from the uncoupled level by an amount

$$W(F,I,J,A,B) = AK/2+B \frac{[3/4\ K(K+1)-I(I+1)\ J(J+1)]}{[2I\ (2I-1)\ J\ (J-1)]} \qquad (3.2)$$

with $K = F(F+1)-I(I+1)-J(J+1)$ [Klu 77].

Identification of the hfs peaks calls for the evaluation of the A and B coefficients (one pair for each J level of the transition). The peaks have been identified on fig. 3.4 a); the next chapter will show in more detail the data analysis.

Figure 3.5 a) shows a close-up view of the Kr^{78} and Kr^{80} peak region to show the sensitivity of the technique. Better statistics are obtained by summing a large number of peaks. Figure 3.5 b) shows the same region as above on a spectrum made of the summation of 16 single scans. In this case the total scan width is only 1.5 GHz thus giving more points per peak. It was made in the hope of getting a very precise value for the Kr^{80}-Kr^{82} IS to remove some ambiguity in the results obtained from wider scans.

The resonance-like shape of the peaks is due to the selection of a relatively large angle (2°) away from

perfect crossing of the two polarisers. The parameters of the equation (2.15) describing these spectra are found using a specially written fitting program. A fit is shown overlapping the data on fig., 3.5 b).

3.2.2) Enriched Kr^{78}.

A sample of Kr enriched up to 99% in Kr^{78} is used. It was mixed in different proportions to natural Kr. Figure 3.6 a) shows a spectrum obtained for a mixture of about 20 % Kr^{78} and 80 % natural Kr. Figure 3.6 b) shows concentrations of 14 % Kr^{78} and 86 % natural Kr. These relative concentrations were deduced from mixing of gas pressures. Note on these spectra the low intensity of the Kr^{80} peak compared to its neighbors. Precise positioning of the Kr^{80} transition cannot be done on these because its peak is shifted by the tails of the two intense adjacent ones. On such scans the Kr^{78}-Kr^{82} shift is obtained, and the Kr^{80}-Kr^{82} shift is found from the natural Kr spectrum; from these two shifts the Kr^{78}-Kr^{80} shift is then known.

Figure 3.4
a) 5.6 GHz scan of natural Kr

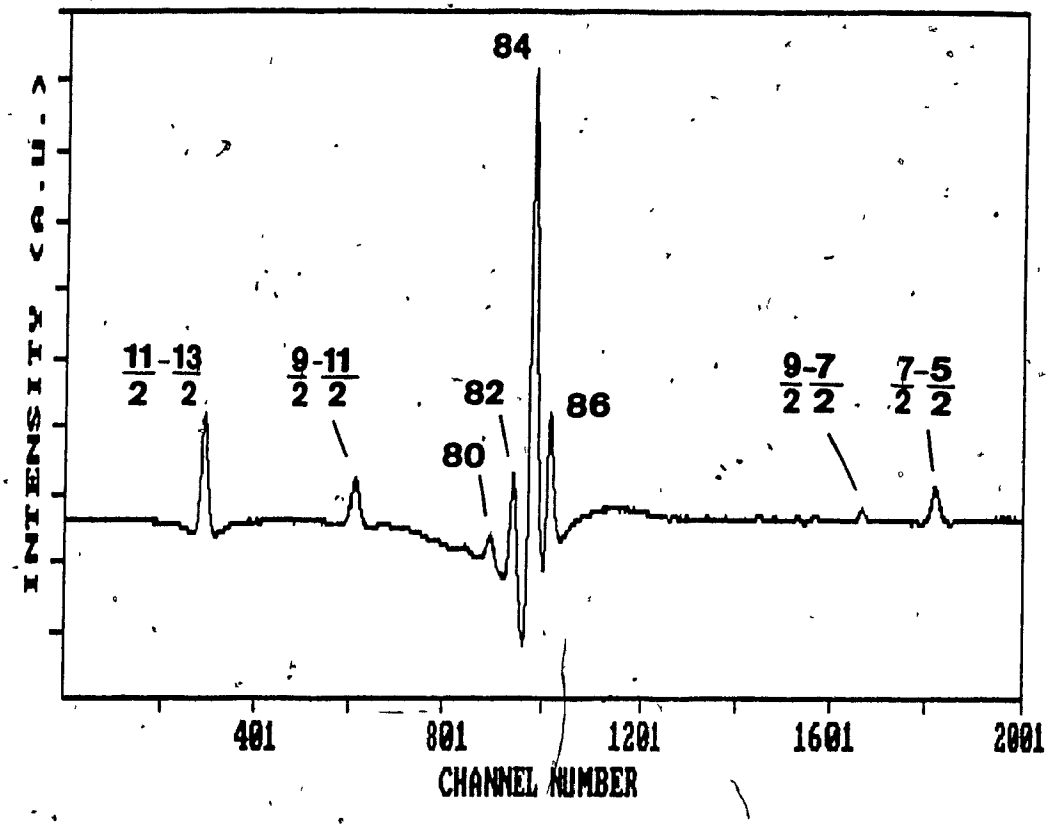

b) etalon spectrum

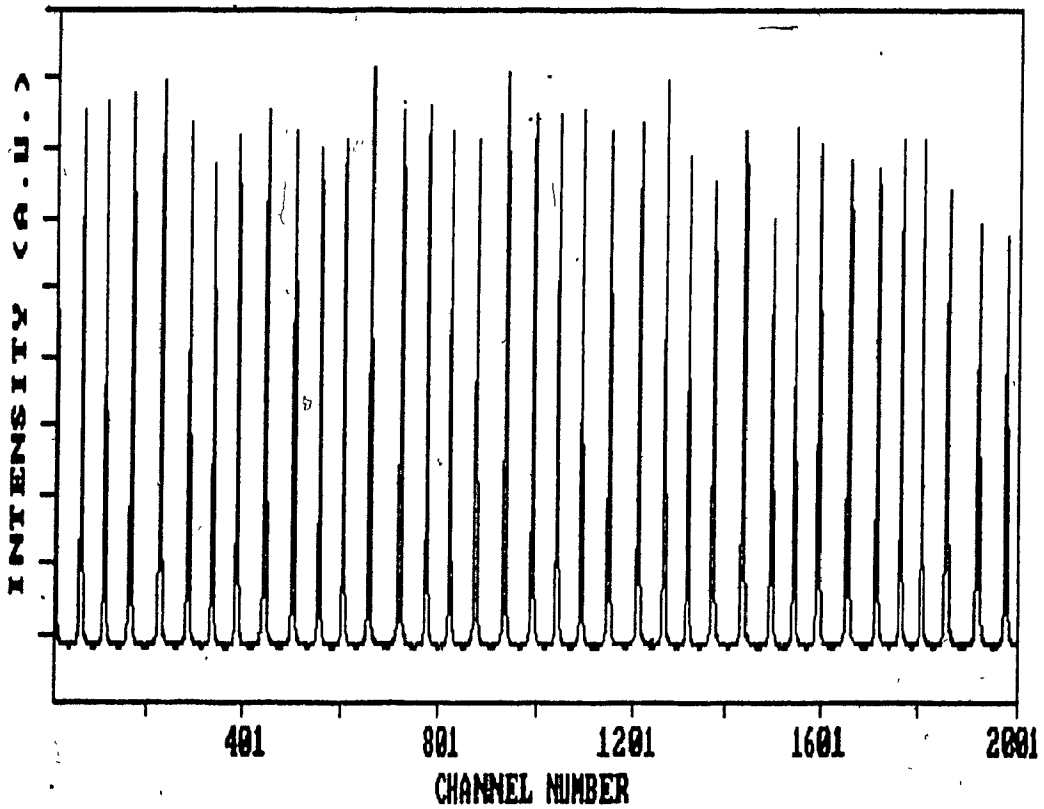

Figure 3.5

a) close up of Kr^{78}_Kr^{80}

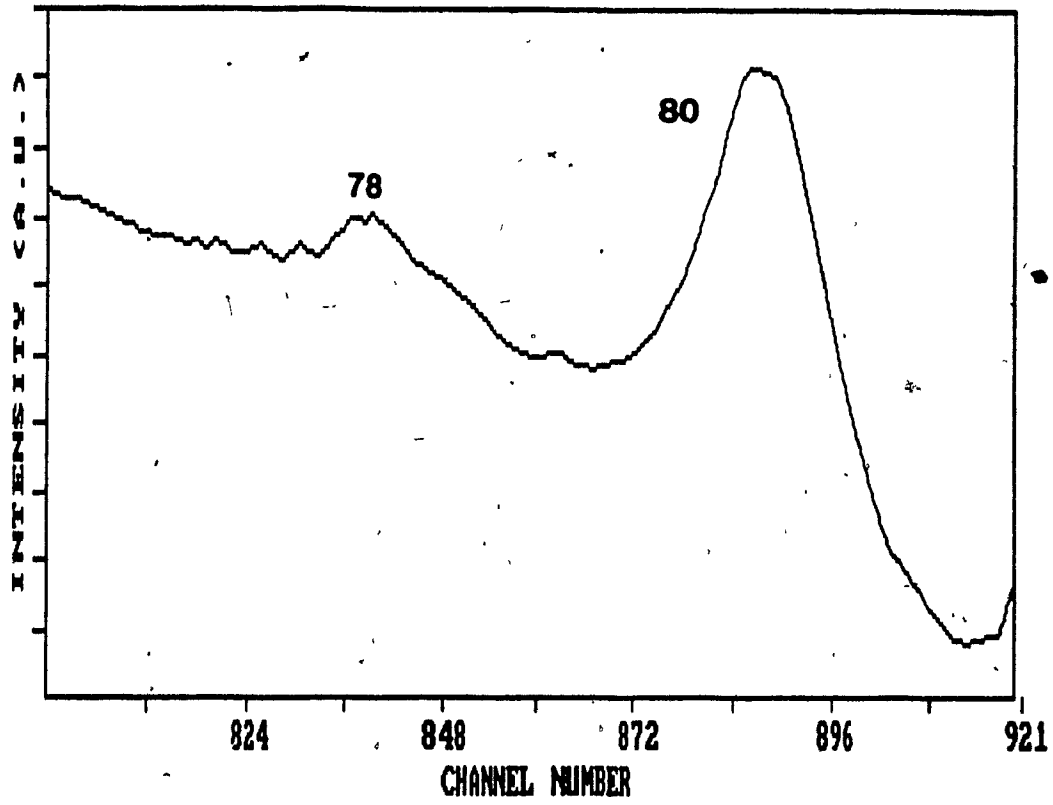

b) other close up

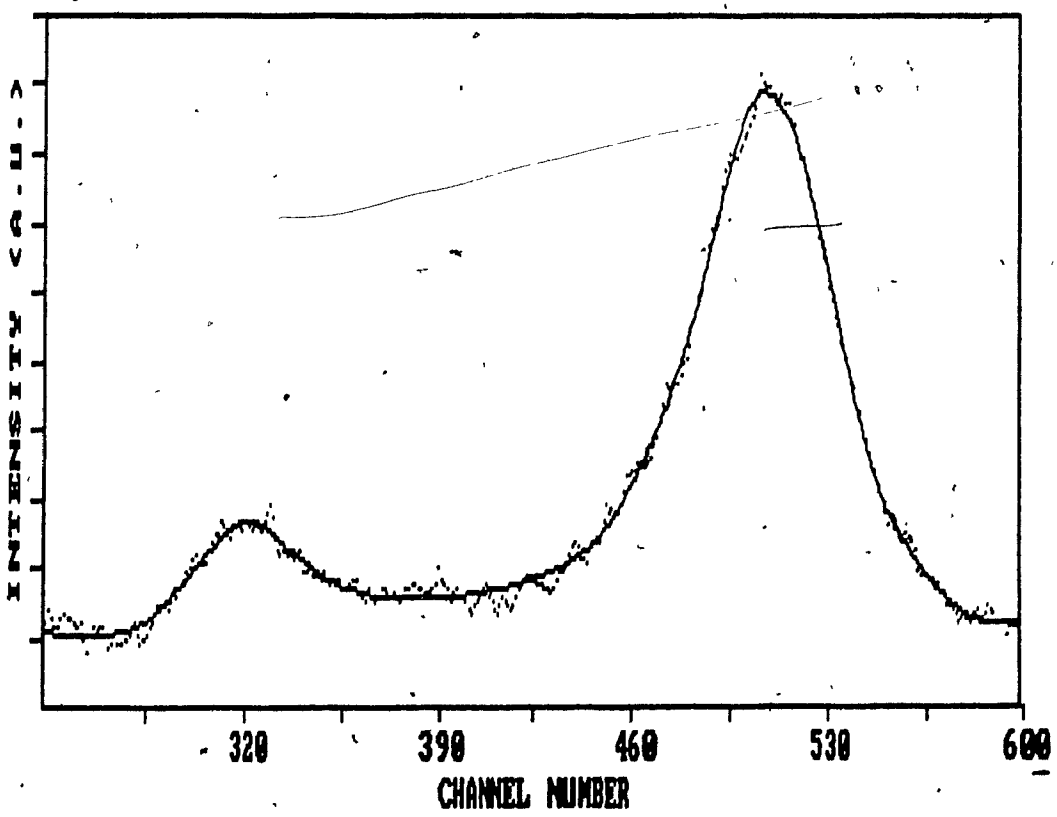

Figure 3.6 Enriched Kr^{78} spectra.

a)

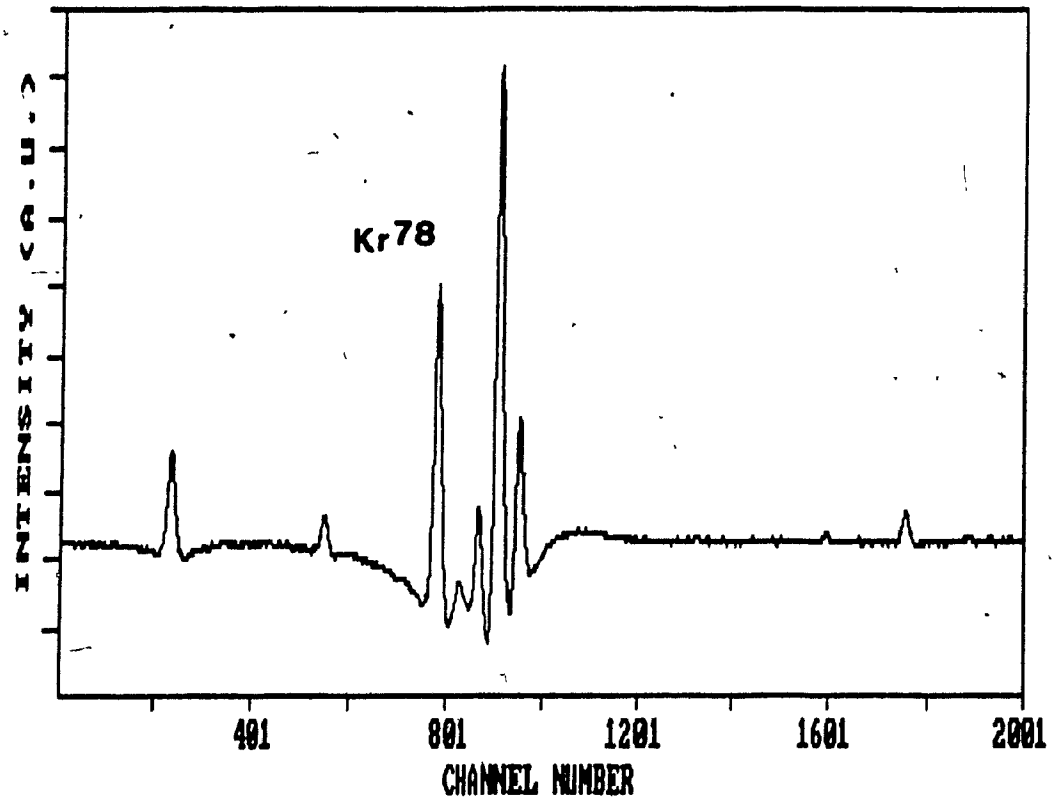

b)

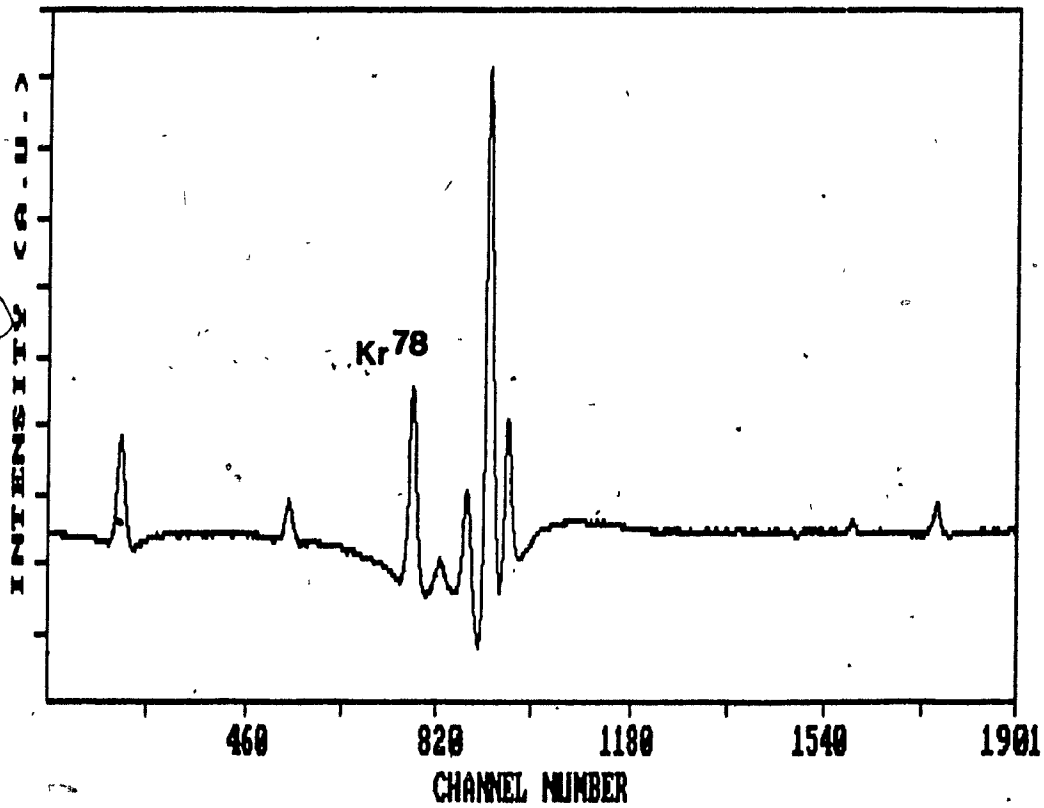

3.3) Spectrum analysis

3.3.1) Doppler-broadened absorption profile.

The shape of the polarisation spectrum is given in part by equation (2.15). Another effect must be taken into account. The probe beam gives a signal when its polarisation axis is slightly rotated due its interaction with a saturated group of atoms whose velocity component along the beam axis is close to zero. This probe beam however is not immune to Doppler broadened absorption at frequencies other than the transition frequency. This absorption curve follows a Gaussian profile, or:

$$I(\omega) = I_o \exp[-(c(\omega-\omega_o)/\omega_o v_p)^2], \qquad (3.3)$$

with $v_p=(2kT/M_A)^{1/2}$.

However, the frequency "ω" at which an atom will absorb the laser photon is dependent on the lifetime of the absorbing transition. The frequency response of the atom is represented by a Lorentzian profile. As mentioned in the previous description of absorption spectroscopy, the overall absorption profile is given by a convolution of the Gaussian and Lorentzian functions;

$$I(\omega) = C\int_0^{\infty} \frac{\exp[-(c(\omega_o-\omega')/\omega_o v_p)^2]}{(\omega-\omega')^2+(\gamma/2)^2}\, d\omega' \; . \qquad (3.4)$$

The shape of this absorption curve is further complicated by the fact that at the center of the spectrum we have not one, but four or five closely spaced transition frequencies. Equation (3.4) gives a familiar inverted bell-shaped curve. However due to frequency modulation we get the derivative as shown in figure 3.7 a). This was obtained by deliberately blocking the pump beam and unbalancing the signal and reference probe beams. Proper balancing of the two probes may somewhat flatten out this curve. In practice however, this effect always remained present. Figures 3.8 a) and b) show the peaks of the even isotopes sitting on absorption backgrounds of different shapes.

If the lifetime of the transition is short, then the linewidth is large and (3.3) suffices to describe the background. In the fitting procedure the background is approximated with:

$$(3.5) \qquad dI(\omega)/d\omega = C_1 \exp[-(\omega_1-\omega)^2/C_2] \, (\omega_1-\omega) + C_3 \, .$$

The "dummy" frequency ω_1 should be centered around the Kr^{84} peak since this transition should contribute the most to the background. C_2 characterizes the linewidth and should be large since it is hoped that (3.5) describes the absorption curve of the five closely spaced transitions. Figure 3.7 b) shows the fit of figure 3.7 a) to equation

(3.5). As expected the fit is only approximate, but is very good in the central portion where the polarisation peaks will appear.

3.3.2) Fitting procedure.

The equation to be fitted to the spectrum is:

$$(3.6)\quad I(\omega) = \sum_i [A_i(1-x_i^2)-2B_i x_i^2]/(1+x_i^2)^2 + C_i \exp[-(\omega_i-\omega)^2/C_2]\,(\omega_i-\omega)+C_3$$

with $x_i = (\omega_{\vartheta,i}-\omega)/\gamma$.

The sum is over the number of peaks present in the region to be fitted. Each peak is determined by four parameters and the background is determined by four parameters as well. Because of the complexity of the equation and the proximity of the peaks one may not determine the center of a transition by simple observation. Thus a fitting program called FITKR3 based on the subroutine CURFIT by Bevington [Bev 69] has been written. It employs a least squares fitting procedure in which all the parameters are searched simultaneously towards a minimum chi-square. Many fits have been done on every spectrum to test the consistency of the parameters found and to help in the estimation of errors. The fitting program is discussed in appendix B.

A fit of the Kr^{78}–Kr^{80} region has already been shown on fig. 3.5. The fig. 3.9 displays the fit of the central portion of the scan. Figure 3.10 shows the point by point subtraction of the fit to the data to demonstrate the goodness of the fit. The reliability of a fit is assessed in many ways: there must be a maximum overlap of the fit to the data, the parameter C_3 describing the constant vertical offset must be constant for all the fitted regions of a given spectrum and the line width found must be realistic. Typically one finds line widths of 35 to 40 MHz, which is very good considering that the laser line width is 20 MHz.

The parameter of most importance is $\omega_{o,i}$ corresponding to the channel position of the i^{th} peak of the fit. The isotope shift between peaks "i" and "j" may then be determined from $\omega_{o,i}-\omega_{o,j}$ and the calibration given by the etalon spectrum. A 5.6 GHz wide scan over 2048 channels gives a calibration of typically 2.780 +/- 0.025 MHz/channel.

Each spectrum gave a set of isotopic shifts, with errors based on the reproducibility of the fits. The final results and errors are averages of results and errors from individual spectra; the fitting routine gave underestimated errors. The Kr^{84}–Kr^{86} and Kr^{82}–Kr^{84} shift results are based on six multiple scans, the Kr^{80}–Kr^{82} results are based on three multiple scans and finally two spectra gave consistent Kr^{78}–Kr^{82} shift values.

Figure 3.7

a) Derivative of the Voigt profile.

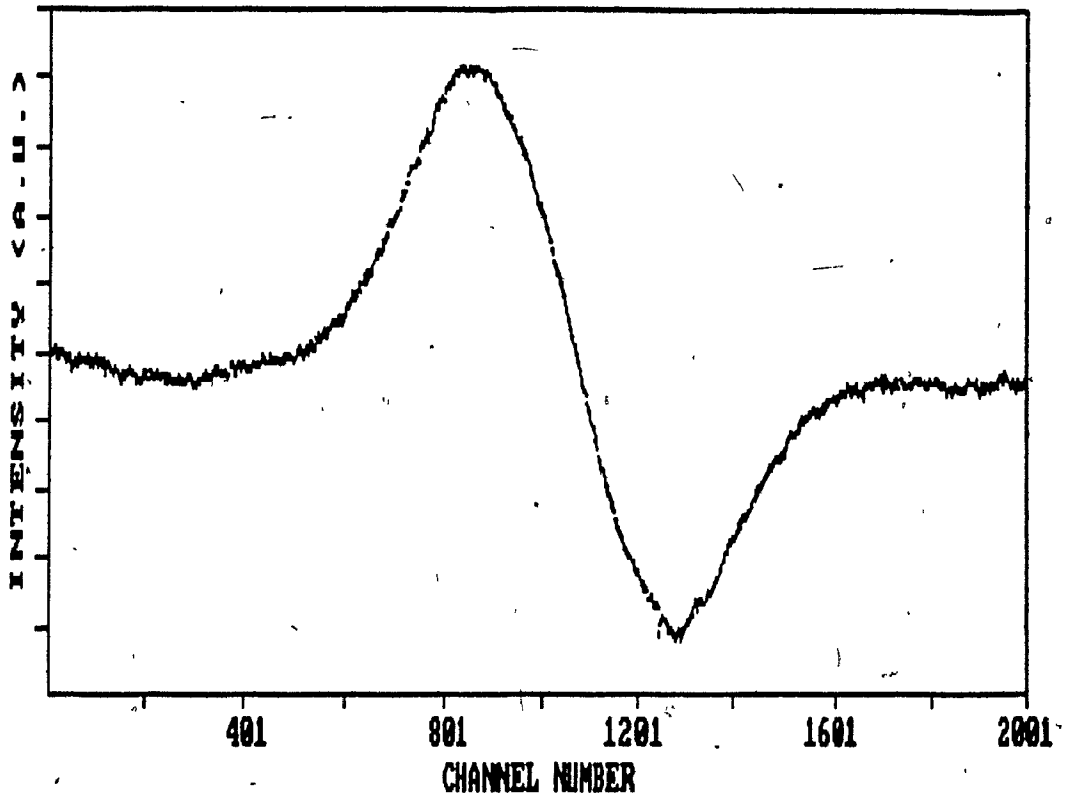

b) Fit

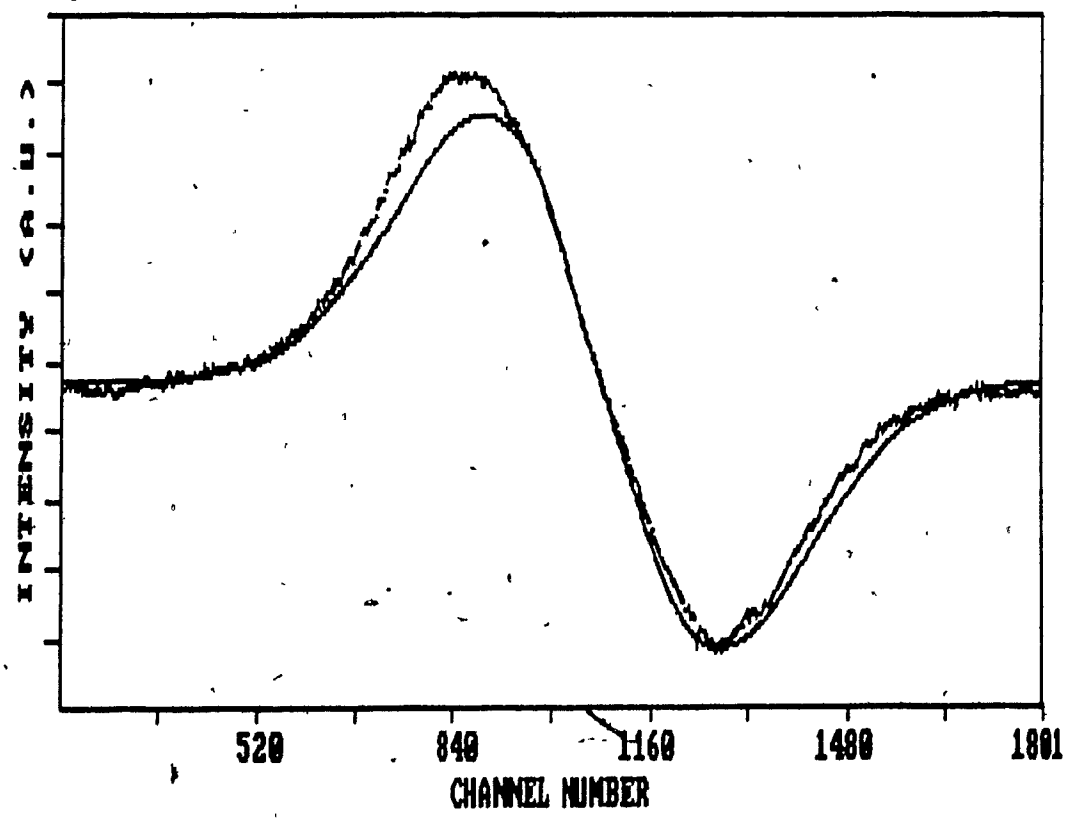

Figure 3.8 Even isotope peaks over different backgrounds.

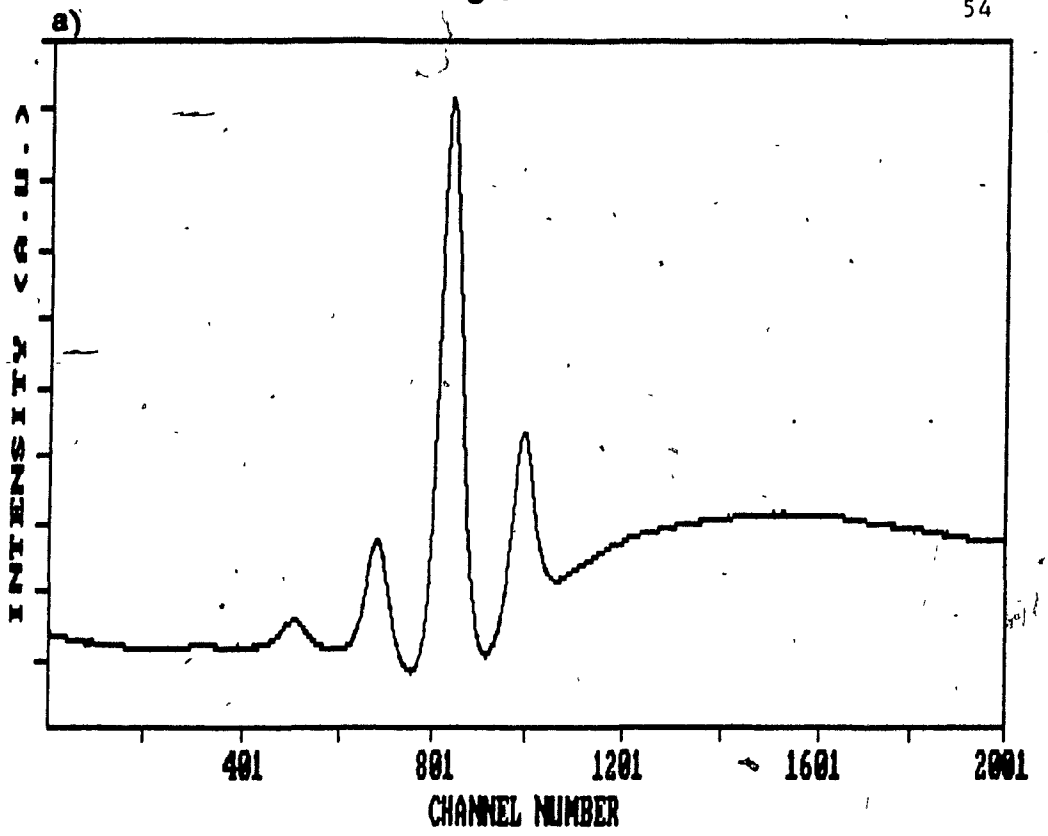

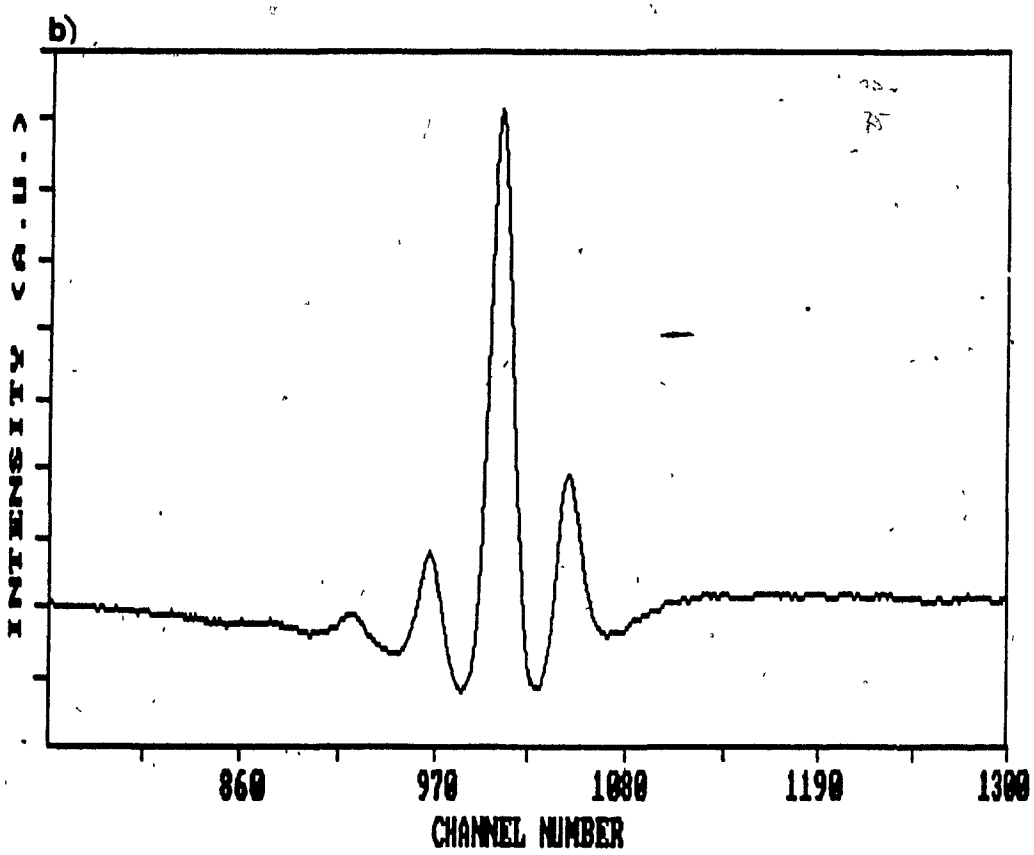

Figure 3.9 Fit of the even isotope peaks.

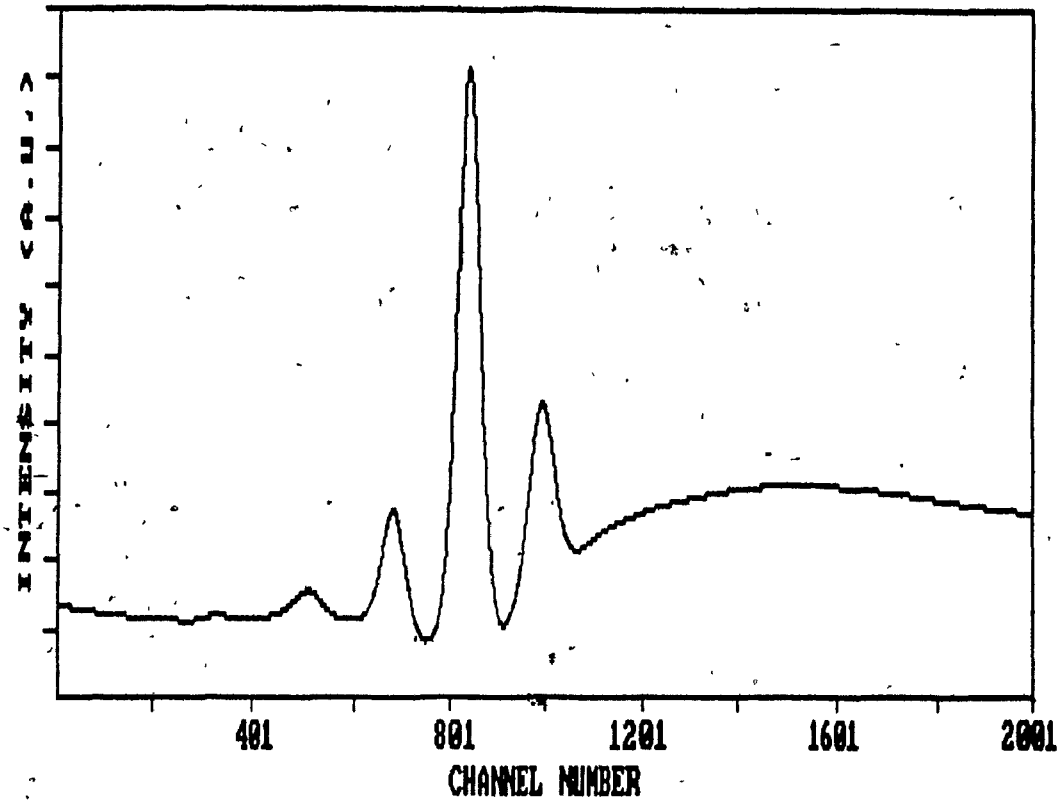

Figure 3.10 Point by point subtraction of the data and fit.

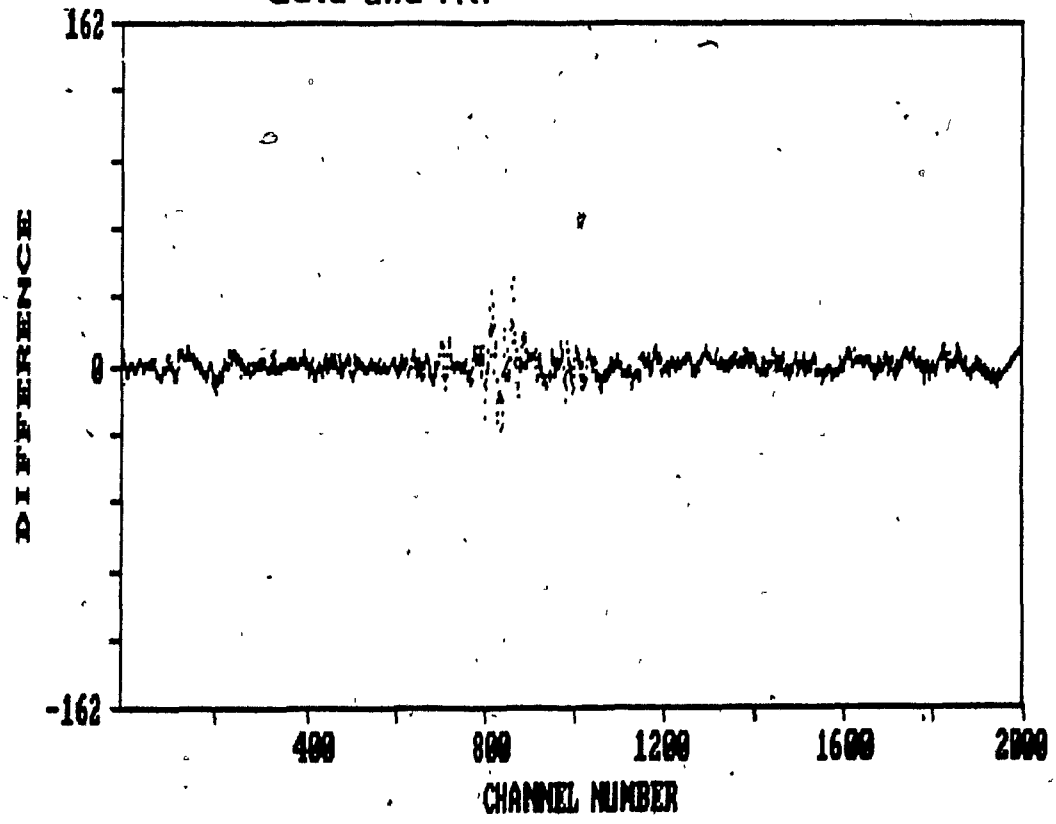

3.3.3) Sensitivity of the technique.

Figure 3.5 b) shows that very weak peaks may be observed by summing a very large number of individual scans; the peak on the left is Kr^{78} of 0.35% abundance and the other is Kr^{80} of 2.27% abundance. The relative sizes of these peaks set a lower detection limit of about 0.1% . The ideal gas equation gives an estimate of the density of atoms required

(3.6) $$= n/V = P/RT\ N_A .$$

For: P= 40mTorr = 5.33 Pa
T= 300 °K

we find: $n = 1.3 \times 10^{13}$ atoms/cc ,

which is the density of atoms giving the desired operating pressure. Thus, a Kr isotope present in a density of 1.3×10^{12} atoms/cc will give a detectable signal. The probe beam volume inside the cell is estimated to be 2 cc and the cell and adjacent valves and tubing volume is roughly 16 cc; 3×10^{12} atoms of any Kr isotope in the beam (i.e. 2×10^{13} atoms in the cell) will give a sizable peak.

From these numbers one finds that 8 mCi of radioactive Kr^{78} mixed with 40 mTorr of natural Kr are required to measure the shift of this isotope. This amount is within the reach of the production reaction $Br^{79}(p,4n)$ for long bombardment times. Thus, the present set- up gives the possibility of spectroscopy on radioactive isotopes of moderate lifetimes, i.e. a few hours.

Chapter 4: Data analysis and results

Finally, this chapter will show the results obtained from the series of spectroscopic measurements performed. The first section is on isotopic shift. The contributions of the three effects to the total shift will be examined and $\delta\langle r^2\rangle$ evaluated for four isotope pairs. The results are to be compared with those obtained by Jackson [Jac 80]. In the second part, the A and B hyperfine structure coefficients of the upper level of the transition will be derived enabling the identification of the peaks of the spectrum shown on figure 3.4 a).

4.1.1) Isotopic shift results.

Each spectrum gave a set of isotopic shifts, with errors reflecting the reproducibility of the parameters generated by the fitting program. The final results and errors are averages from individual spectra. The resulting Kr^{84}-Kr^{86} shift value is based on six multiple scans, while the Kr^{80}-Kr^{82} result comes from three multiple scans, one of them being the sum of 16 single scans. Two enriched Kr^{78} spectra give the Kr^{78}-Kr^{82} shift and so the Kr^{78}-Kr^{80} shift is determined.

Table 4.1 displays the total shifts, the

calculated normal mass shifts, the residual shift (FS+SMS) and the modified residual shifts. The modified shifts are calculated using

(4.1) $$\delta\nu^{AA'}{}_{587,FS+SMS} = \frac{M_{84-86}}{M_{AA'}}\,\delta\nu^{AA'}{}_{587,FS+SMS} ,$$

and displayed on a King plot.

Table 4.1: Kr isotope shifts (in MHz) for the 587 nm line.

peaks	$\delta\nu^{total}$	$\delta\nu^{NMS}$	$\delta\nu^{FS+SMS}$	$\delta\nu'^{FS+SMS}$
78-80	131.3 +/- 3.3	89.9	41.4 +/- 3.3	35.8 +/- 2.9
80-82	125.8 +/- 2.2	85.5	40.3 +/- 2.2	36.6 +/- 2.0
82-84	115.9 +/- 1.9	81.4	34.5 +/- 1.9	32.9 +/- 1.8
84-86	112.4 +/- 1.8	77.6	34.8 +/- 1.8	34.8 +/- 1.8

First evidence of a volume effect is given on graph 4.1 where the total shifts are plotted with respect to the normal mass shift. Without volume effects the total shift is strictly proportional to $M_{AA'}$ for a given transition, as shown by:

(4.2) $$\delta\nu^{AA'}{}_{i,total} = M_{AA'}\,[M_{i,NMS}+M_{i,SMS}] + F_i\,\delta^{AA'}\langle r^2\rangle ,$$

which is equation (1.25) rearranged. Departure from linearity is due to a non-zero field shift term, i.e. a non-zero $\delta^{AA'}\langle r^2\rangle$. The graph shows greater than expected

shifts in the lightest isotopes.

Table 4.2 shows the Kr IS measurements for the 557 nm line obtained by Gerhardt [Ger 79].

Table 4.2: Kr isotope shifts (in MHz) for the 557 nm line.

peaks	$\delta\nu^{total}$	$\delta\nu^{NMS}$	$\delta\nu^{FS+SMS}$	$\delta\nu'^{FS+SMS}$
78-80	102.3 +/- 0.8	94.0	8.3 +/- 0.8	7.2 +/- 0.7
80-82	94.6 +/- 0.8	89.4	5.2 +/- 0.8	4.7 +/- 0.7
82-84	84.6 +/- 0.6	85.1	-0.5 +/- 0.6	-0.47+/- 0.5
84-86	87.5 +/- 0.6	81.2	6.3 +/- 0.6	6.3 +/- 0.6

Plotting the modified shifts of the 587 nm line versus those of the 557 nm line yields a King plot. A straight line is expected as predicted by (1.27). Its slope gives F(587)/F(557), and the offset is:

$$M_{84-86}\,[\,M(587)^{SMS} - F(587)/F(557)\;M(557)^{SMS}\,]\;.$$

The 557 nm transition data is used because the electronic factor F(557) is known and is equal to -0.54 GHz fm^{-2}, with no error given [Ger 79].

The King plot is shown on graph 4.2. Its slope is found to be 0.36 +/- 0.17 which gives F(587)= -0.19 +/- 0.09 GHz fm^{-2}. A theoretical estimate of $\delta^{84-86}\langle r^2\rangle$ has been done and gave $-(32.1 +/- 20.1)\times10^{-3}$ fm^{-2} [Ger 79]. We now have all the required information to calculate the SMS contribution to the total shift and $\delta^{\wedge\wedge'}\langle r^2\rangle$ for all the

isotope pairs. The following equations are used:

(4.3) a) $\delta\nu^{84-86}_{587,SMS} = \delta\nu^{84-86}_{587,SMS+FS} - F(587)\ \delta^{84-86}\langle r^2\rangle$

b) $\delta\nu^{AA'}_{587,SMS} = M_{AA'}/M_{84-86}\,\delta\nu^{84-86}_{587,SMS}$

c) $\delta^{AA'}\langle r^2\rangle = (\delta\nu^{AA'}_{587,SMS+FS} - \delta\nu^{AA'}_{587,SMS})/F(587)$

The results are listed in table 4.3.

Table 4.3: SMS for the 587 nm line and $\delta^{AA'}\langle r^2\rangle$

peak	$\delta\nu^{AA'}(587)_{SMS}$ (MHz)	$\delta^{AA'}\langle r^2\rangle$ ($\times 10^{-3}$ fm^2)
78-80	32.9 +/- 6.0	-40.2 +/- 32.9
80-82	31.3 +/- 5.7	-50.0 +/- 40.2
82-84	29.8 +/- 5.4	-24.2 +/- 32.0
84-86	28.4 +/- 5.2	-32.7 +/- 20.1

4.1.2) Isotopic shift results - Jackson [Jac 80]

For comparison the following results obtained by Jackson in 1980 are listed. These are used rather than Audet's [Aud 85] because they include measurements of the Kr^{78}-Kr^{80} shifts. Table 4.4 displays the total shift, FS+SMS, and the modified residual shift. The NMS are the same as the ones given in table 4.1.

Table 4.4: Kr IS of the 587 nm line - Jackson [Jac 80]

peaks	$\delta\nu^{total}$	$\delta\nu^{FS+SMS}$	$\delta\nu'^{FS+SMS}$
78-80	133.5 +/- 3.3	43.6 +/- 3.3	37.7 +/- 2.9
80-82	124.2 +/- 3.0	38.7 +/- 3.0	35.1 +/- 2.7
82-84	114.0 +/- 3.0	32.6 +/- 3.0	31.1 +/- 2.9
84-86	113.1 +/- 1.5	35.5 +/- 1.5	35.1 +/- 1.5

Jackson's modified residual shifts plotted as a function of the 557 nm shifts from Gerhardt yield a King plot of slope 0.78 +/- 0.26. This gives an electronic factor F(587)= -0.42 +/- 0.14 GHz fm^{-2}. Table 4.5 displays the SMS and the $\delta^{AA'}\langle r^2\rangle$ obtained from these results.

Table 4.5:SMS for the 587 nm line and $\delta^{AA'}\langle r^2\rangle$-Jackson

peaks	$\delta\nu^{SMS}$(MHz)	$\delta^{AA'}\langle r^2\rangle \times 10^{-3}$ fm^2
78-80	25.1 +/- 11.3	-44.0 +/- 31.0
80-82	23.9 +/- 10.8	-35.2 +/- 28.8
82-84	22.8 +/- 10.3	-23.3 +/- 26.6
84-86	21.7 +/- 9.8	-32.7 +/- 20.1

Graph 4.1 Total shift versus specific mass shift

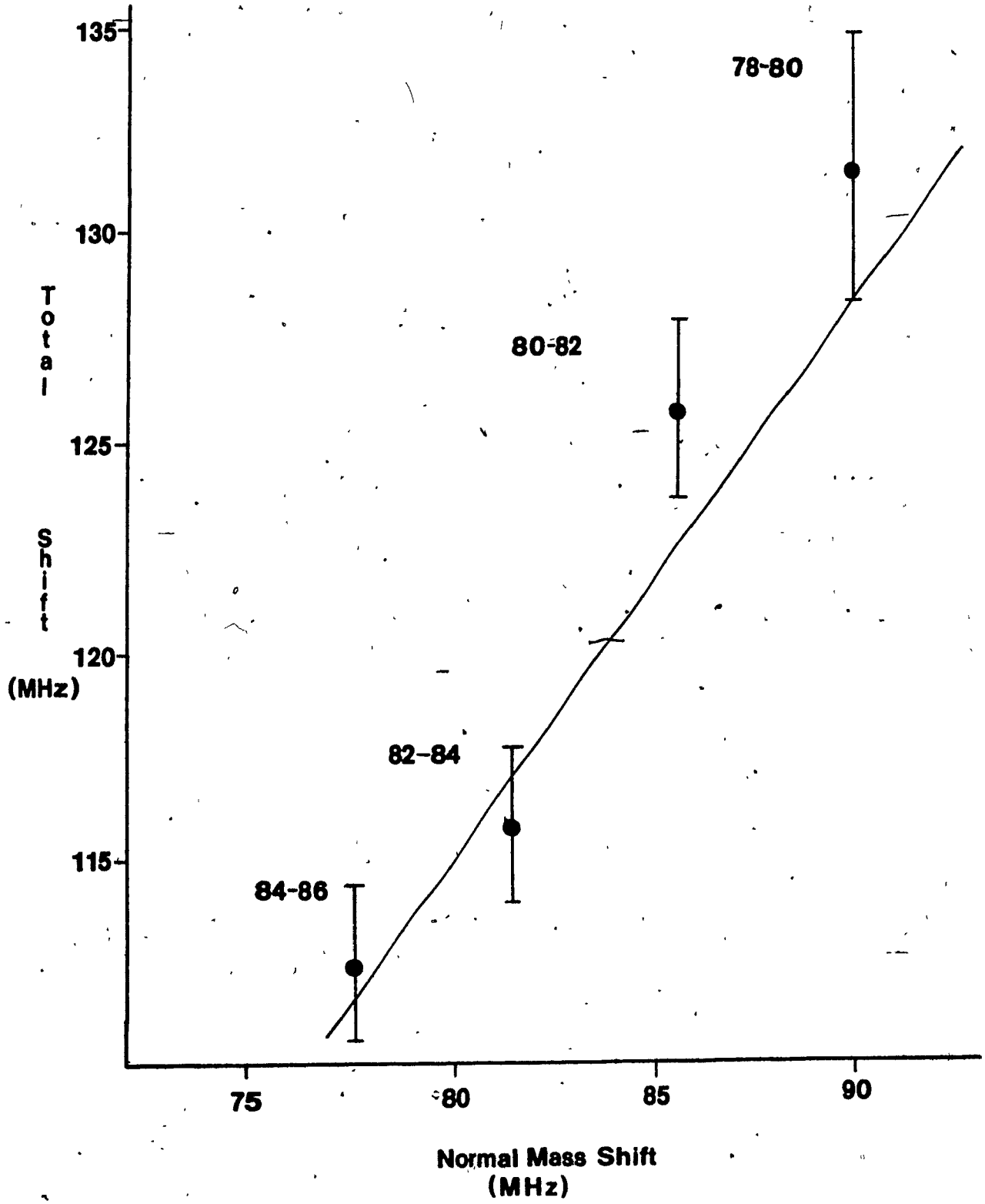

Graph 4.2 King Plot

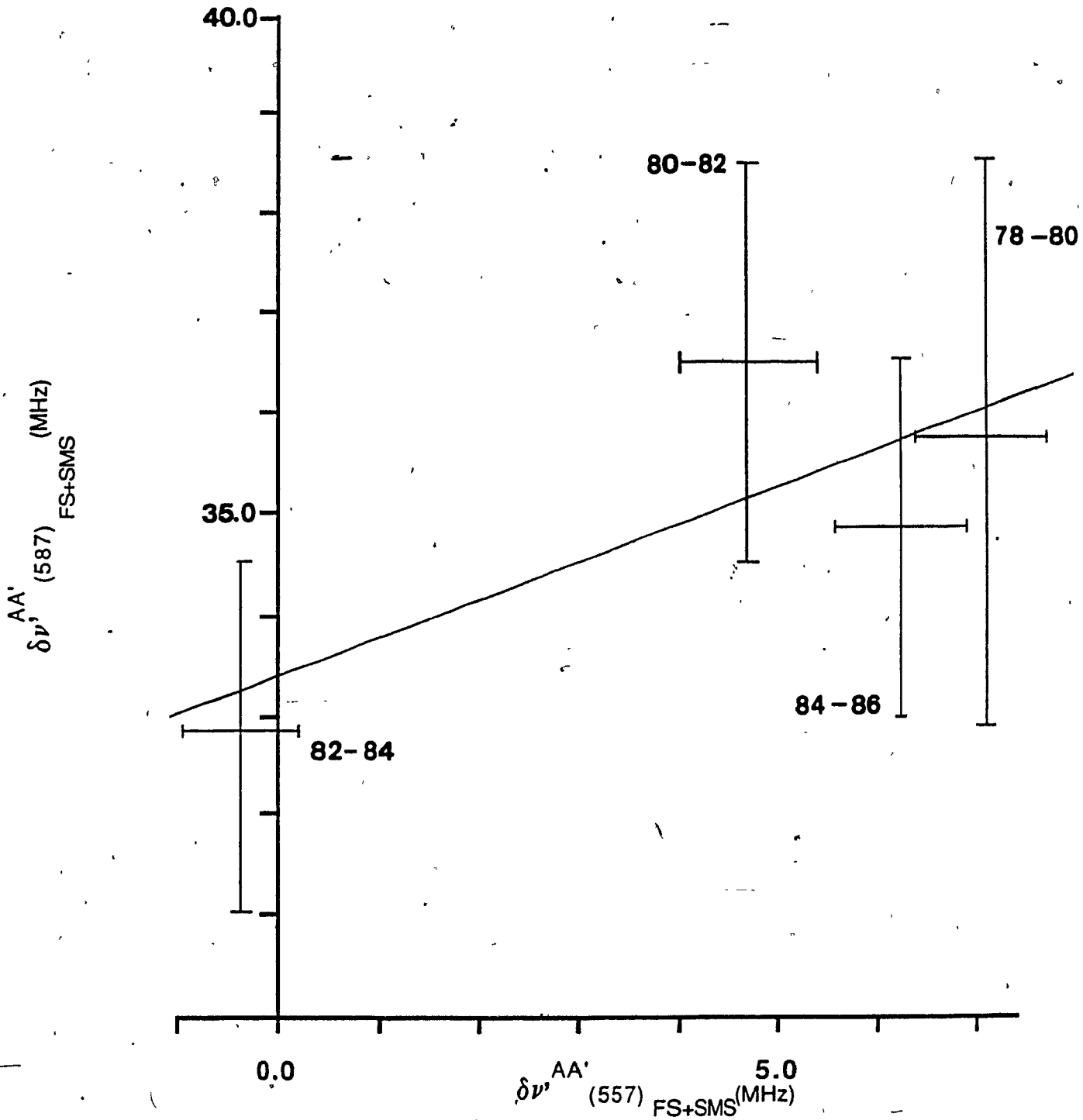

4.1.3) Discussion of the results

The results of the present work confirm the findings of past experiments. The isotopic shifts involving the s level in krypton cannot be due totally to the mass effect: volume effects are present.

Our results for $\delta\nu^{AA'}\langle r^2\rangle$ confirm the observation of Gerhardt who studied the 557 nm transition in 1977 [Ger 77]. Adding neutrons in the lower half of the $g_{9/2}$ shell (A=78 to A=82) introduces the largest change in $\delta\langle r^2\rangle$ compared to filling the upper half (A=82 to 86). This is also observed on graph 4.1 which shows shifts greater than those expected for the Kr^{78}-Kr^{80} and Kr^{80}-Kr^{82} pairs.

As expected the $\delta^{AA'}\langle r^2\rangle$ are negative, as adding neutron pairs brings the number of neutrons close to the magic number. Radioactive Kr^{76} is now believed to be one of the most deformed nuclei in the ground state [Mar 86], while the closed shell Kr^{86} is spherical. Thus, the $\delta^{AA'}\langle r^2\rangle$ give evidence of a change in the nuclear shape from Kr^{76} to Kr^{86}. This gives ample motivation to perform studies of the Kr^{76}-Kr^{78} shift.

The total shifts measured here are in good agreement with those obtained by Jackson. However, the residual shifts $\delta\nu^{78,80,82,84,86}$ are very close for all the isotope pairs. These yield a King plot whose slope seems arbitrary considering the relative magnitude of the errors. The electronic factor obtained here is F(587)= -0.19 +/- 0.09

GHz fm^{-2}, while Jackson's result is -0.42 +/- 0.14 GHz fm^{-2}. This discreptancy is understandable; a difference of only one channel in a shift measured on a spectrum means eventually displacing a point by 2.5 MHz on the King plot. Despite the difference in F(587), the values for the SMS and $\delta^{AA'}\langle r^2\rangle$ agree with Jackson's results. The most that one may realistically hope for is to determine unambiguously the sign of $\delta^{AA'}\langle r^2\rangle$, and estimate the relative contributions of the NMS, SMS and FS to the total shift.

4.2) Hyperfine structure.

On figure 3.4 a) four hfs peaks belonging to Kr^{83} are labelled. In this section, the A_2 and B_2 coefficients of the hyperfine splitting of the upper level will be determined bringing about the identification of all visible hfs peaks. As shown in appendix A, the upper level of the transition 5s[3/2]1-5p'[3/2]2 has five hyperfine sublevels, while the lower transition has three, giving nine allowed transitions. The difference in energy between an upper and a lower sublevel may be written as:

$$E_{21} = E_2+W_{F2}-(E_1+W_{F1}) = E_2-E_1+(W_{F2}-W_{F1}) \qquad (4.4)$$

where E_2 and E_1 are the center of the upper and lower levels, and W_{F1} and W_{F2} are the hyperfine splittings of the

particular sublevels. The quantity E_2-E_1 is the expected transition energy in the absence of hyperfine splitting, which may be assumed to be at the center of the spectrum, i.e. very close to the Kr^{84} peak. The energy $W_{F2}-W_{F1}$ is then the distance of the hfs peak to the Kr^{84} peak.

The A and B coefficients of the splitting of the lower level have been found by Jackson [Jac 77]. They are:

$$A_{J=1} = -160.4 +/- 0.6 \text{ MHz},$$

$$B_{J=1} = -105.9 +/- 0.6 \text{ MHz}.$$

Thus the distance of any hfs peak to the Kr^{84} peak is given by:

$$(4.5)\quad W(I=9/2,J=2,K')-W(I=9/2,J=1,K)=1/2\ K'\ A_2+B_2/432$$
$$[3/4\ K'(K'+1)-148.5]+80.2\ K+1.47[3/4\ K(K+1)-49.5]$$

according to equation (3.2). Audet has done a thorough study of the hfs of Kr^{83} and found the two leftmost peaks to belong to the transition 11/2-13/2 and 9/2-11/2. On our spectrum these peaks are separated from the Kr^{84} peak by -1011 +/- 17 MHz and -1874 +/- 17 MHz respectively. Putting these numbers and the appropriate K values in (4.5) gives A_2=-295.4 MHz and B_2=143.5 MHz.

With these values of A_2 and B_2 the two leftmost peaks may be identified. One could try the remaining seven hyperfine transitions, put the appropriate K values in (4.5) and match the measured separations to the calculated ones. Using some foresight we try the 9/2-7/2 and 7/2-5/2

transitions. Table 4.6 lists the measured and calculated separation of the four hfs peaks to the Kr^{84} peak.

Table 4.6 Kr^{83} to Kr^{84} peak distances (in MHz).

transition	measured	calculated
11/2-13/2	-1874 +/- 17	-1874
9/2-11/2	-1011 +/- 17	-1011
9/2-7/2	1887 +/- 25	1987
7/2-5/2	2337 +/- 30	2491

The two last transitions listed are those which give the best correspondence between the measured and calculated separation. Now that four hfs peaks are identified one may find better values of A_2 and B_2 which do not rely on the assumption that the Kr^{84} peak and the center of gravity of the Kr^{83} transitions coincide. Instead the actual hfs peaks separations are used.

The separation between the two leftmost peaks is 874.5 MHz and yields the equation:

$$-6.5\ A_2 - .542\ B_2 = 1854.3\ \text{MHz}\ .$$

The separation between the two rightmost peaks is 450.5 MHz and yields the equation:

$$-3.5\ A_2 + .437\ B_2 = 1061.6\ \text{MHz}\ .$$

Solving these give A_2=-292.5 MHz and B_2=86.6 MHz. This places the center of the Kr^{83} transitions 53+/-34 MHz to the left of the Kr^{84} peak; i.e. halfway between the Kr^{82}

and Kr^{84} peaks. The high error is a reflection of the high error in the evaluation of the position of the low intensity Kr^{83} peaks (as shown on table 4.6). There is also a large uncertainty associated with the spectrum calibration due to non-linearity in the laser scanning, giving a large cumulative error over wide intervals such as those which characterise hfs.

The other five Kr^{83} peaks lie between the four peaks studied. In Audet's work, the 9/2-9/2 and 7/2-7/2 peaks were clearly visible, but they remain undetected here. However, the 9/2-7/2 peak is found here and was invisible to Audet; the reason for this is not known. One possibility is that the frequency modulation technique favors some peaks over others due to the different form of the $I(\omega)$ spectrum (see equation 3.5)

Conclusion

This work has demonstrated the usefulness of using a double probe beam and frequency modulating the laserr output, as modifications to the technique of polarisation spectroscopy. Perfect elimination of the Doppler-broadened absorption background could not be achieved, but it could be substantially reduced. The frequency modulation gave spectrum and background which are derivatives of the amplitude modulated technique; this complicated somewhat the spectrum intensity equation. Hence, the positioning of the transitions called for a lengthy fitting procedure. However, the sensitivity attained using this background reducing technique allows isotopic shift measurements for isotopes present in concentrations as low as 0.1 % .

Measurements of isotope shifts were done on the stable even Kr isotopes in natural and enriched mixtures. The resulting calculations yielded the separation of the field and the specific mass shifts and the $\delta\langle r^2\rangle$ were found. The enriched mixtures were used to enhance the signal from the less abundant Kr^{78} isotope to improve the precision over previous measurements. Also the A and B hyperfine splitting coefficients of Kr^{83} were determined for the upper level and the center of gravity of the hyperfine transitions was found.

The high sensitivity attained with the present technique should allow the determination of the shift between the radioactive Kr^{76} and the stable Kr^{78} isotopes. This should be most interesting due to the strong deformation of Kr^{76}.

Appendix A: KrI spectra

A.1) Even isotopes

For rare gases L-S coupling does not hold and the excited energy levels must be found on the basis of jl coupling, where j is the angular momentum of the core which has one hole due to the excited electron, and l is the orbital angular momentum of the electron. It turns out that the levels are grouped in pairs with the total angular momentum J varying by one unit. A conventional way to describe a state is nl[K]J, where n and l are the principal and orbital angular momentum quantum numbers of the excited electron, K is the angular momentum obtained from the jl coupling, and may take on the values from $|j+l|$ to $|j-l|$ in unit step. J is the total angular momentum of the state obtained from the vector addition of K and s, the excited electron's spin. For a given "nl" excited state it may happen that this identification scheme yields more than one state of particular K and J values. For this reason the one formed using the lowest j value (hence, highest in energy) is written as nl'[K]J.

In the case of KrI, the ground state is $4p^5\,{}^1S_0$. A first set of excited levels is found from the $4p^55s^1$ group. This leaves a hole in the core having $l_h=1$, $s_h=1/2$ giving $j=3/2,\ 1/2$. The excited electron has l=0 and s=1/2. The core angular momentum j=3/2 couples with l to give the states;

$5s[3/2]2$ and

$5s[1/2]1$.

The angular momentum j=1/2 gives the primed states;

$5s'[1/2]1$ and

$5s'[1/2]0$.

The second group of excited levels are from the group $4p^5 5p^1$, and it is now easy to show that the following states are obtained;

with j=3/2;

$5p[5/2]3$ $5p[5/2]2$

$5p[3/2]2$ $5p[3/2]1$

$5p[1/2]1$ $5p[1/2]0$ and

with j=1/2;

$5p'[3/2]2$ $5p'[3/2]1$

$5p'[1/2]1$ $5p'[1/2]0$.

The energy level diagram is shown on figure A.1; The 557 nm line correspondig to the $5p'[3/2]2$-$5s[3/2]2$ transition and the 587 nm line corresponding to the $5p'[3/2]2$-$5s[3/2]1$ transition are shown.

A.2) Hyperfine splitting of the 587 nm line of Kr^{86}

The last neutrons in Kr fill the $g_{9/2}$ shell. Kr^{86} has one unpaired neutron and thus possesses a nuclear spin I=9/2. An electronic level of angular momentum J has the hyperfine sublevels given by F=J+I. Hence, the upper level

of the 587 nm transition has the hyperfine sublevels 13/2,11/2,9/2,7/2,5/2, and the lower level has the sublevels 11/2,9/2,7/2. The nine allowed transitions obey the selection rules F=0,+/-1. They are shown in figure A.2 . The ones which show up on the polarisation spectrum are the 11/2-13/2 and 9/2-11/2 on the left, and 9/2-7/2 and 7/2-5/2 on the right of the even isotope peaks.

Fig. A.1: Energy levels of the $4p^5 5s^1$ and $4p^5 5p^1$ groups of Kr I.

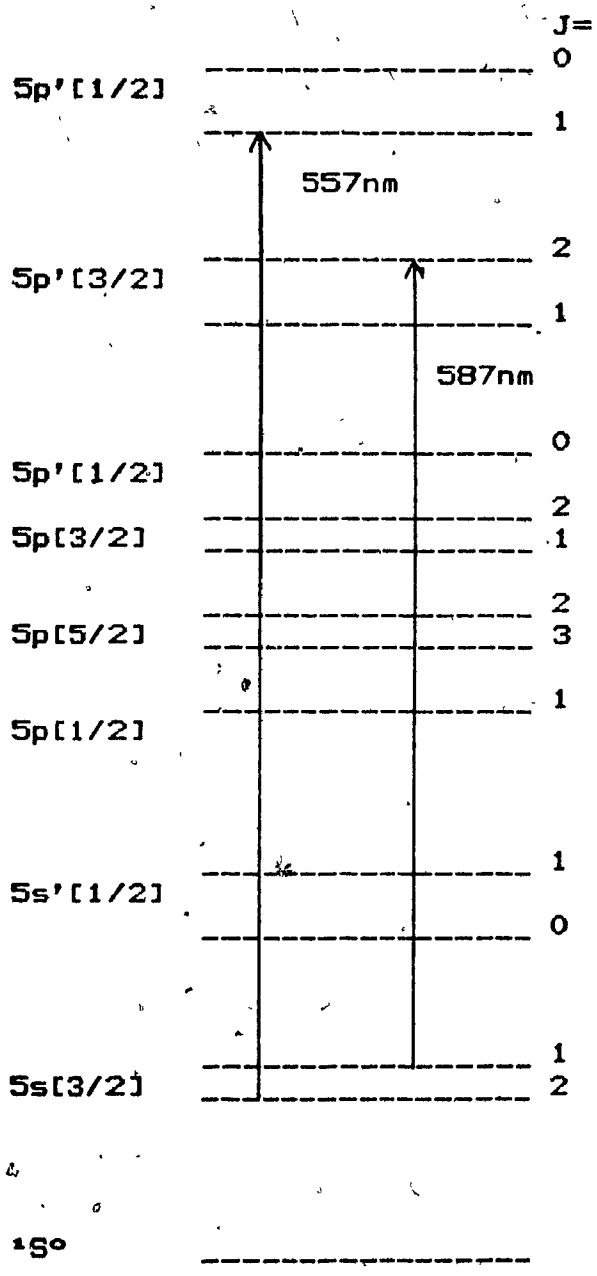

Fig. A.2: Hyperfine transitions of Kr^{83}.

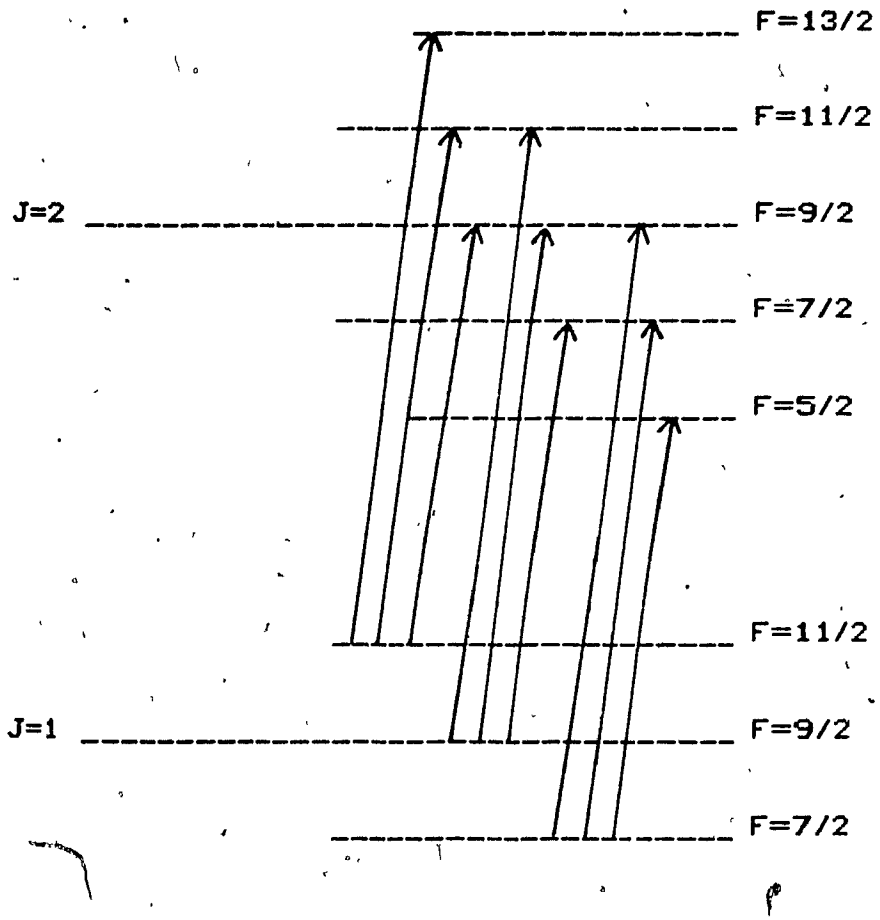

Appendix B: Programs

A few programs have been specially written to analyse and display the spectrum. Little will be said about the display program except that it is based on a graphics subroutine package called HALO [HAL- 85]. The program, written in FORTRAN, allows the overlay of two spectra, which shows its usefulness when data and fits are compared. The etalon calibration and the spectrum fitting programs are described next in greater detail.

B.1) Etalon calibration program

The listing of the etalon calibration program, called FPEAK, is given at the end of this appendix. Its purpose is to find the average etalon peak separation and to find the calibration using the known mode spacing. It relies first on a lower threshold parameter , LOTH, and considers every channel whose content is greater than LOTH as being part of a peak. The peak's boundaries are defined by the first channel on the left to the last channel on the right which are above the threshold. After a peak has been found, its centroid is calculated (lines 72 to 75).

When all points have been analysed and a set of peaks have been found, the intervals between all the peaks

must be greater than a user-specified lower limit (line 104). Closely spaced peaks are considered as multiple peaks caused by the frequency modulation of the laser and a weighted average center is found (lines 105 and 106). Finally, the average interpeak separation and average deviation from the mean are found, giving the spectrum calibration and error using the etalon mode spacing.

B.2) The spectrum fitting program

The fitting procedure consists of a main program and three related subroutines. They are:

FITKR2; main program which handles data input/output and the parameter search,

MATINV; matrix inversion subroutine found in Bevington [Bev 69],

FCHISQ; subroutine to calculate χ^2, also from [Bev 69],

FUNCTN2; function subprogram containing the polarisation equation to fit to the data.

FITKR2 is based on a parameter search subroutine called CURFIT written by Bevington. It does a simultaneous search of all the parameters of the equation to be fitted through the minimization of the χ^2. Following is a description of the fitting procedure.

Call y(i) the function to be fitted and y_i the data in channel "i". The function y(i) depends on the

parameters a_j to be found. The function may be expanded to first order in the parameters;

$$(b.1) \qquad y(i)=y_o(i)+\sum_{j=1}^{nPARA}\left[\partial y_o(i)/\partial a_j\ \delta a_j\right] ,$$

where the sum is over the number of parameters. The problem boils down to evaluating the δa_j's to bring the function close to the data. To do this the χ^2 is minimized with respect to the parameter increments δa_j's;

$$(b.2) \qquad \chi^2=\sum_{i}^{NPoints} 1/\sigma_i^2\left[y_i-y_o(i)-\sum_{j}^{nPARA}\left[\partial y_o(i)/\partial a_j\ \delta a_j\right]\right]^2 \quad ;$$

$$(b.3) \qquad \partial\chi^2/\partial\delta a_k=-2\sum_{i} 1/\sigma_i^2\left[y_i-y_o(i)-\sum_{j}\left[\partial y_o(i)/\partial a_j\ \delta a_j\right]\right]$$
$$\partial y_o(i)/\partial a_k \ = 0 .$$

This yields a matrix equation in δa_j's;

$$(b.4) \qquad \beta_k=\sum_{j}^{nPARA.}\delta a_j\ \alpha_{jk} \quad \text{with}$$

$$(b.5) \qquad \beta_k=\sum_{i}^{Npoints} 1/\sigma_i^2\ (y_i-y_o(i))\ \partial y_o(i)/\partial a_k$$

$$\alpha_{jk}=\sum_{i}^{Npoints} 1/\sigma_i^2\ \partial y_o(i)/\partial a_j\ \ \partial y_o(i)/\partial a_k .$$

The FITKR2 requires starting input parameters. The first χ^2 is calculated and minimized giving the set of n equations. These yield simultaneously increments to all the parameters which are put back in the function to be fitted, and a new χ^2 is found. To accelerate the parameter search

and prevent divergence, a special feature is used to vary the direction of the search in parameter space. The matrix equation (b.4) is rewritten as;

(b.6) $$\beta_k = \sum_{j=1}^{n} a_j \, \alpha_{jk} \, (1+\delta_{jk}\lambda) \quad .$$

The parameter λ determines the search direction. If it is large the matrix equation becomes n separate equations:

(b.7) $$\beta_j = \lambda \, \delta a_j \, \alpha_{jj}$$

which gives increments δa_j in the direction of the gradient $\partial y_o(i) / \partial a_j$. In successive iterations, if the χ^2 increases, is multiplied by 10 to accelerate the convergence. If the χ^2 decreases, then λ is divided by 10 to slow down the search and prevent divergence. Other schemes to vary λ may be used and the successfulness of a fit on this scheme and on the initial input values of λ and a_j's.

Now examine the FITKR2 program. The data and initial parameters are read in lines 60 to 118. Then the σ_i's (WEIGHT(I)) are evaluated from lines 122 to 136. In lines 142 to 173 the β_k's and α_{jk}'s are evaluated calling upon the subprogram FUNCTN2. In lines 155 to 162, the partial derivatives of the function with respect to the parameters are found. At line 182, the initial χ^2 is calculated. The matrix $\bar{\alpha}$ is inverted at line 197 and the new

parameters are found at line 205. These are put back in the function at line 216. If the new χ^2 is greater than the old one, λ is multiplied by 10 and new parameters are found. If the new χ^2 is smaller, the new parameters become the input parameters to the fit, λ is divided by 10 and a new iteration begins. When the χ^2 decreases by less than a user-specified tolerance value, or when the number of iterations have reached a preset upper limit, the resultant parameters are put in a formatted file (lines 246 to 266) and the fit to the data is saved (line 272).

The MATINV and FCHISQ subroutine have been borrowed unaltered from Bevington [Bev 69]. The FUNCTN2 function subprogram contains the derivative of the polarisation spectrum intensity equation (2.15).

```
D Line# 1      7                                  Microsoft FORTRAN77 V3.20 02/84
      1 C      Program FPEAK used to analyse the etalon spectrum. It
      2 C      finds the center of gravity of each peak, finds the
      3 C      number of peaks, the mean interpeak distance and the
      4 C      mean square deviation from this mean. The program
      5 C      prompts the user for the etalon spacing and thus cali-
      6 C      brates the spectrum. The program eliminates spurious
      7 C      peaks which are usually below a certain threshold spe-
      8 C      cified by the user. The printout will contain the mean
      9 C      interpeak distance and its error and the positions of
     10 C      the peaks. The following integer variables are used:
     11 C               X(2048)= array of channel contents
     12 C             LOTH= lowwer threshold value
     13 C             WAREA= weighted area (sum of chan.# * content)
     14 C             APEA= sum of channel content within a peak
     15 C      The following real variables are used:
     16 C             DIF(60)= array containing interpeak distances
     17 C             AVIN= average interpeak distance
     18 C        ETSP= mode spacing of the etalon in MHz
     19 C        ETEP= error on ETSP
     20 C        CAL= calibration
     21 C        EPCAL= error on the calibration
     22 C        CMX(60)= array containing the cm of each peak.
     23 C      The TOLerance refers to the width in channels within
     24 C      which multiple peaks should considered as making up
     25 C      a single peak and be averaged. The choice of LOTH and
     26 C      TOL must be optimised to give the smallest error.
     27 C
     28        REAL DIF(60),CMX(60),AVIN,SMEAN,ETSP,ETEP,CAL,EPCAL,EPPOP,
     29       $     FLOAT,TOL
     30        INTEGER*4 X(4096),LOTH,WAREA(60),APEA(60)
     31        CHARACTER*1 ANS1,ANS2
     32        CHARACTER*20 DUMMY,PEAK
     33 C
     34        WRITE(*,50)
     35 1      CONTINUE
     36        WRITE(*,100)
     37        READ(*,1100) DUMMY
     38        OPEN(UNIT=1,FILE=DUMMY,STATUS='OLD',FORM='BINARY')
     39        WRITE(*,150)
     40        READ(*,*) N
     41 C
     42 C      NOW READ ALL THE DATA FROM THE ETALON FILE INTO X(N).
     43 C
     44        READ(1) (X(I),I=1,N)
     45        CLOSE(1)
     46 3      CONTINUE
     47        WRITE(*,200)
     48        READ(*,*) LOTH
     49        WRITE(*,225)
     50        READ(*,*) TOL
     51        WRITE(*,*) 'MARKER 1'
     52        J=1
     53        I=1
     54        DO 2 K=1,60
     55        APEA(K)=0
     56        WAREA(K)=0
     57 2      CONTINUE
     58 C
     59 C      IN THE FOLLOWING LOOPS THE ETALON DATA IS EXAMINED. IF A
```

```
      C     PEAK IS FOUND ITS CM IS CALCULATED. THIS IS DONE UNTIL I=N.
      C
      C     THE FOLLOWING TEST IS DONE TO ENSURE THAT WE DO NOT START
      C     IN THE MIDDLE OF A PEAK.
    4 CONTINUE
      IF (X(I) .GT. LOTH) THEN
        I=I+1
        GO TO 4
      ENDIF
    5 CONTINUE
      IF (I .GE. N) GO TO 8
      IF (X(I) .GT. LOTH) THEN
        WAREA(J)=WAREA(J)+(X(I)-LOTH)*I
        AREA(J)=AREA(J)+X(I)-LOTH
         IF (X(I+1) .LE. LOTH) THEN
         CMX(J)=FLOAT(WAREA(J))/FLOAT(AREA(J))
          I=I+1
         J=J+1
         GO TO 5
       ELSE
         I=I+1
      GO TO 5
        ENDIF
      ELSE
      I=I+1
      GO TO 5
      ENDIF
      C
      C     WE NOW HAVE THE FOLLOWING; J-1 PEAKS FOUND, CMX( )
      C     WHICH CONTAINS THE J-1 PEAK POSITIONS.
      C
    8 J=J-1
      WRITE(*,*) 'MARKER 2'
      IF (J .EQ. 0) THEN
        WRITE(*,250)
        GO TO 60
      ENDIF
      C
      C     THE FOLLOWING LOOP DETERMINES IF THE PEAKS ARE SINGLE
      C     OR MULTIPLE PEAKS.
      C
      L=1
   85 CONTINUE
      WRITE(*,*) L
      IF ((CMX(L+1)-CMX(L)) .LE. TOL) THEN
        CMX(L)=(CMX(L+1)*FLOAT(APEA(L+1))+CMX(L)*FLOAT
     $  (APEA(L)))/(AREA(L+1)+APEA(L))
        AREA(L)=APEA(L)+APEA(L+1)
        DO 97 I=L+1,J-1
         CMX(I)=CMX(I+1)
          APEA(I)=APEA(I+1)
   97   CONTINUE
        J=J-1
       IF (L .EQ. J) GO TO 96
        L=L-1
      ENDIF
      L=L+1
      IF (L .LE. (J-1)) GO TO 85
   96 CONTINUE
```

```
D Line# 1      7                          Microsoft FORTRAN77 V3.20 02/84
     119 *       WRITE(*,*) 'MARKER 3'
     120 C
     121 C       NOW CALCULATE THE AVERAGE INTERPEAK DISTANCE
     122 C
     123         AVIN=(CMX(J)-CMX(1))/FLOAT(J-1)
     124         DO 10 I=1,J-1
1    125           DIF(I)=CMX(I+1)-CMX(I)
1    126 10      CONTINUE
     127         DIF(J)=0
     128 C
     129 C      CALCULATE THE MEAN SQUARE DEVIATION.
     130 C
     131         WRITE(*,*) 'MARKER 4'
     132         SMEAN=0
     133         DO 20 I=1,J-1
1    134         SMEAN=SMEAN+(DIF(I)-AVIN)**2
1    135 20      CONTINUE
     136         ERROR=SQRT(SMEAN)/FLOAT(J-2)
     137 C
     138 C      READ IN THE ETALON SPECIFICATIONS.
     139 C
     140         WRITE(*,300)
     141         READ(*,*) ETSP,ERSP
     142         CAL=ETSP/AVIN
     143         ERCAL=CAL*(ERROR/AVIN+ERSP/ETSP)
     144 C
     145         WRITE(*,400)
     146         READ(*,1100) PEAK
     147         OPEN(UNIT=2,FILE=PEAK,STATUS='NEW',FORM='FORMATTED')
     148 C       ENTER RESULTS IN THE OUTPUT FILE.
     149         WRITE(2,525) PEAK,DUMMY
     150         WRITE(2,450) AVIN,ERROR
     151         WRITE(2,710) ETSP,ERSP
     152         WRITE(2,500) CAL,ERCAL
     153         WRITE(2,505) TOL
     154         WRITE(2,510) LOTH
     155         WRITE(2,550)
     156         WRITE(2,600) (I,CMX(I),DIF(I),I=1,J)
     157         CLOSE(2)
     158 C
     159 C       DO AGAIN ?
     160         WRITE(*,650)
     161         READ(*,1500) ANS1
     162         IF (ANS1 .EQ. 'N') GO TO 60
     163           WRITE(*,700)
     164         READ(*,1500) ANS2
     165         IF (ANS2 .EQ. 'Y') THEN
     166           DUMMY='
     167           GO TO 1
     168         ELSE
     169           GO TO 3
     170         ENDIF
     171 C
     172 C       WRITE FORMATS:
     173 C
     174 50      FORMAT('0','THIS PROGRAM WORKS FOR A MAX OF 60 ETALON PEAKS',/)
     175 100    FORMAT(' ENTER THE ETALON FILENAME :',/)
     176 150    FORMAT(' ENTER THE # OF CHANNELS (2048,4096):',/)
     177 200    FORMAT(' ENTER THE LOWER THRESHOLD :',/)
```

```
D Line# 1      7                                  Microsoft FORTRAN77 V3.20 02/84
     178 225    FORMAT(' ENTER PEAK RESOLUTION IN # OF CHANNELS:',/)
     179 250    FORMAT(' NO PEAKS WERE FOUND ABOVE THRESHOLD',/)
     180 300    FORMAT(' ENTER INTERMODE SPACING, ERROR IN MHz:',/)
     181 400    FORMAT(' ENTER OUPUT FILENAME :',/)
     182 450    FORMAT(' THE MEAN PEAK SEPARATION IS ',F7.3,1X,
     183       $       'WITH AN ERROR OF ',F5.3,' CHANNELS',/)
     184 500    FORMAT(' THE SPECTRUM CALIBRATION IS ',F6.3,2X,
     185       $       'WITH AN ERROR OF ',F5.3,' MHZ/CHAN',/)
     186 505    FORMAT(' THE TOLERANCE IS ',F3.0,' CHANNELS',/)
     187 510    FORMAT(' THE THRESHOLD IS ',I4,' COUNTS',/)
     188 525    FORMAT('0',10X,A7,4X,A7,/)
     189 550    FORMAT('0',10X,'PEAK NO.',5X,'PEAK POSITION',7X,'INTERVAL',
     190       $  /,' ',10X,'********',5X,'**************',7X,'********',/)
     191 600    FORMAT(' ',13X,I2,10X,F8.3,11X,F8.3)
     192 650    FORMAT(' ANOTHER TRY (Y/N) ?')
     193 700    FORMAT(' READ A NEW ETALON SPECTRUM (Y/N) ?',/)
     194 710    FORMAT(' INTERMODE SPACING IS ',F6.2,' +/- ',
     195       $       F4.2,' MHZ',/)
     196 C
     197 C      READ FORMATS:
     198 C
     199 1100   FORMAT(A20)
     200 1500   FORMAT(A1)
     201 C
     202 60      STOP
     203         END
```

Name	Type	Offset	P	Class
ANS1	CHAR*1	17458		
ANS2	CHAR*1	17459		
AREA	INTEGER*4	17106		
AVIN	REAL	17402		
CAL	REAL	17430		
CMX	REAL	16866		
DIF	REAL	2		
DUMMY	CHAR*20	17346		
ERCAL	REAL	17434		
ERROR	REAL	17418		
ERSP	REAL	17426		
ETER	REAL	*****		
ETSP	REAL	17422		
FLOAT				INTRINSIC
I	INTEGER*4	17370		
J	INTEGER*4	17386		
K	INTEGER*4	17390		
L	INTEGER*4	17394		
LOTH	INTEGER*4	17378		
N	INTEGER*4	17366		
PEAK	CHAR*20	17438		
SMEAN	REAL	17410		
SQRT				INTRINSIC
TOL	REAL	17382		
WAREA	INTEGER*4	16626		
	INTEGER*4	242		

D Line# 1 7 Microsoft FORTRAN77 V3.20 02/84

```
      $NOFLOATCALLS
C     Program FITKR to fit the IS spectrum over
C     a predetermined range and find the centers
C     a maximum of 7 peaks.
C     Based on the subroutine CUPFIT by Bevington
C     and on MANFIP by Audet.
C     Complementary subroutines:
C          FUNCTN=parameter dependent equation of
C           the spectrum to be fitted
C           FCHISQ=finds chi-square of the function
C           MATINV=matrix inversion program.
C     FITKR prompts the user for the channel interval
C     to be fitted and the starting parameters. The
C     chi-square is then calculated. The minimisation
C     to first order of the chi-square gives NTERMS
C     equations with an equal number of unknowns. The
C     matrix is inverted and new parameters are found.
C     The program looks for the best parameters in the
C     parameter space in steps size set by FLAMDA.
C
C     Real variables:
C         A(NTERMS)=parameter array
C          DELTAA(NTERMS)=interval array for derivative
C          SIGMAA(NTERMS)=parameter error array
C          B(NTERMS)=new parameter array
C          DERIV(NTERMS)=partial derivative array
C          YFIT(NPTS)=fitted spectrum array
C          FLAMDA=parameter space search step size
C          CHISQ1=initial chi-square
C          CHISQT=test chi-square
C         CHISQ=final chi-square
C         WEIGHT(NPTS)=statistical weight of each data pt
C     for chi-square minimisation:
C          BETA(NTERMS)
C          ALPHA(NTERMS,NTERMS)
C          ARRAY(NTERMS,NTERMS)=inverted ALPHA matrix
C
C     Integer variables:
C          N1,N2=fitting range in channels
C          NPTS=number of data pts
C          NTERMS=number of fitting parameters
C          NFREE=number of degrees of freedom
C          ICOUNT=number of iterations
C          Y(1000)=data pts array
C          IDUM( )=dumping array
C     Character variables:
C          FILN1=data filename
C          FILN2=fitted parameter filename
C          FILN3=fitted spectrum filename
C
      CHARACTER*20 FILN1,FILN2,FILN3,ANS*1
      REAL FLOAT,A(29),FLAMDA,YFIT(1000),SIGMAA(29)
      REAL DELTAA(29),ALPHA(29,29),BETA(29),B(29),DERIV(29)
      DOUBLE PRECISION ARRAY(29,29),DIFF,CHISQ1,CHISQ
      DOUBLE PRECISION CHISQT,WEIGHT(1000)
      INTEGER N1,N2,NPTS,NTERMS,NFREE,ICOUNT
      INTEGER*4 IDUM(2048),Y(1000),IFIX
C
C     INPUT DATA
```

D Line# 1 7 Microsoft FORTRAN77 V3.20 02/84

```
      C
            WRITE(*,*) 'ENTER THE SPECTRUM FILENAME:'
            READ(*,100) FILN1
  100       FORMAT(A20)
            OPEN(UNIT=1,FILE=FILN1,ACCESS='SEQUENTIAL',STATUS='OLD',
     $         FORM='BINARY')
            REWIND(1)
            WRITE(*,*) 'CURVE TO BE FITTED FROM ,TO (IN CHANNELS)?'
            READ(*,*) N1,N2
            NPTS=N2-N1+1
      C
      C     READ IN Y(I) ONLY THE PTS TO BE FITTED
      C
            READ(1) IDUM
            DO 6 I=1,NPTS
      1     Y(I)=IDUM(I+N1-1)
      1   6 CONTINUE
            CLOSE(1)
      C
      C     ENTER THE VARIOUS PARAMETERS
      C
            WRITE(*,*) 'ENTER THE NUMBER OF PEAKS TO BE FITTED (MAX 7):'
            READ(*,*) NTERMS
            NTERMS=NTERMS*4+4
            WRITE(*,*) 'ENTER THE NUMBER OF OFFSET COUNTS:'
            READ(*,*) A(NTERMS-3)
            IC=1
            DO 10 I=1,NTERMS-7,4
            WRITE(*,*) 'ENTER A,D,W,GAMMA OF PEAK # ',IC
            READ(*,*) A(I),A(I+1),A(I+2),A(I+3)
      1     A(I+2)=A(I+2)+1.-FLOAT(N1)
      1     IC=IC+1
      1   10 CONTINUE
            WRITE(*,*) ' '
            WRITE(*,*)    'THE DOPPLER BROADENED ABSORPTION IS GIVEN'
            WRITE(*,*)    'BY C1*EXP(-1*(I-W1)**2/C2)*(I-W1). ENTER'
            WRITE(*,*)    'C1,C2,W1:'
            READ(*,*) A(NTERMS-2),A(NTERMS-1),A(NTERMS)
            A(NTERMS)=A(NTERMS)-N1+1
            WRITE(*,*) 'ENTER THE CHISQ TOLERANCE (TOL > 1):'
            READ(*,*) TOL
      C
      C     OUTPUT FILENAMES:
      C
            WRITE(*,*) 'ENTER THE FINAL PARAMETER FILENAME:'
            READ(*,100) FILN2
            WRITE(*,*) 'ENTER THE FITTED SPECTRUM FILENAME:'
            READ(*,100) FILN3
      C
      C     SET INITIAL FLAMDA AND WEIGHTS
      C
      7     WRITE(*,*) 'ENTER THE NUMBER OF ITERATIONS:'
            READ(*,*) NITS
            ICOUNT=1
            WRITE(*,*) 'ENTER STARTING VALUE OF FLAMDA (.0001 ?):'
            READ(*,*) FLAMDA
            NFREE=NPTS-NTERMS
            IF (NFREE .LE. 0) THEN
            WRITE(*,*) 'THERE IS NO DEGREE OF FREEDOM'
```

```
D Line# 1     7                          Microsoft FORTRAN77 V3.20 02/84
     119          GO TO 800
     120          ENDIF
     121 C
     122 C        THE WEIGHTS ARE EVALUATED STATISTICALLY AND THE
     123 C        NUMBER OF COUNTS IS TAKEN AS THE NUMBER AWAY FROM
     124 C        THE OFFSET.
     125 C
     126 16       CONTINUE
     127          II=0
     128          CHISQT=0.
     129          IF (ICOUNT .GT. 10) GO TO 25
     130          LC=IFIX(A(NTERMS-3)+.5)
     131          DO 15 I=1,NPTS
   1 132          IF (Y(I) .NE. LC) THEN
   1 133          WEIGHT(I)=1./ABS(FLOAT(Y(I)-LC))
   1 134          ELSE
   1 135          WEIGHT(I)=1.
   1 136          ENDIF
   1 137 15       CONTINUE
     138 C
     139 C        CALCULATE THE DERIVATIVES SUMMED OVER ALL PTS
     140 C        (MODIFICATION OF BEVINGTON'S FDERIV)
     141 C
     142 25       DO 17 J=1,NTERMS
   1 143          BETA(J)=0.
   1 144          DO 17 K=1,J
   2 145          ALPHA(J,K)=0.
   2 146 17       CONTINUE
     147 C
     148          DO 38 J=1,NTERMS
   1 149          DELTAA(J)=ABS(A(J)/100.)
   1 150 38       CONTINUE
     151 C
     152 C        EVALUATE THE MATRICES
     153 C
     154          DO 50 I=1,NPTS
   1 155          DO 42 J=1,NTERMS
   2 156          AJ=A(J)
   2 157          A(J)=A(J)+DELTAA(J)
   2 158          YYFIT=FUNCTN2(I,A,NTERMS)
   2 159          A(J)=AJ-DELTAA(J)
   2 160          DERIV(J)=(YYFIT-FUNCTN2(I,A,NTERMS))/(2.*DELTAA(J))
   2 161          A(J)=AJ
   2 162 42       CONTINUE
   1 163          DO 46 J=1,NTERMS
   2 164          BETA(J)=BETA(J)+WEIGHT(I)*(FLOAT(Y(I))-FUNCTN2
   2 165         $(I,A,NTERMS))*DERIV(J)
   2 166          DO 46 K=1,J
   3 167          ALPHA(J,K)=ALPHA(J,K)+WEIGHT(I)*DERIV(J)*DERIV(K)
   3 168 46       CONTINUE
   1 169 50       CONTINUE
     170          DO 53 J=1,NTERMS
   1 171          DO 53 K=1,J
   2 172          ALPHA(K,J)=ALPHA(J,K)
   2 173 53       CONTINUE
     174 C
     175 C        IF THIS IS THE FIRST ITERATION, FIND THE STARTING
     176 C        VALUE OF CHISQ.
     177 C
```

D Line# 1 7 Microsoft FORTRAN77 V3.20 02/84

```
     178          IF (ICOUNT .EQ. 1) THEN
     179          DO 54 I=1,NPTS
     180 54       YFIT(I)=FUNCTN2(I,A,NTERMS)
     181          CALL FCHISQ(Y,WEIGHT,NPTS,NFREE,YFIT,CHISQ)
     182          CHISQ1=CHISQ
     183          ENDIF
     184          WRITE(*,*) 'CHISQ1 FOUND'
     185          WRITE(*,*) 'CHISQ1=',CHISQ1
     186 C
     187 C        NORMALISE ALPHA AND INVERT USING MATINV ROUTINE
     188 C
     189 71       CONTINUE
     190          DO 74 J=1,NTERMS
   1 191          DO 73 K=1,NTERMS
   2 192          ARRAY(J,K)=ALPHA(J,K)/SQRT(ALPHA(J,J)*ALPHA(K,K))
   2 193 73       CONTINUE
   1 194          ARRAY(J,J)=1.+FLAMDA
   1 195 74       CONTINUE
     196 C
     197          CALL MATINV(ARRAY,NTERMS,DET)
     198          WRITE(*,*) 'ALPHA INVERTED'
     199 C
     200 C        EVALUATE THE NEW PARAMETERS AND CALL THEM B(I)
     201 C
     202          DO 84 J=1,NTERMS
   1 203          B(J)=A(J)
   1 204          DO 84 K=1,NTERMS
   2 205          B(J)=B(J)+BETA(K)*ARRAY(J,K)/SQRT(ALPHA(J,J)*ALPHA(K,K))
   2 206 84       CONTINUE
     207 C
     208 C        PUT THESE PARAMETERS IN THE FUNCTION. IF THE NEW CHISQ IS
     209 C        GREATER THAN THE PREVIOUS ONE THE SEARCH PARAMETER FLAMDA
     210 C        IS MULTIPLIED BY 1 OR 10. IF IT IS SMALLER FLAMDA IS DIVIDED
     211 C        BY 10.
     212 C
     213          DO 92 I=1,NPTS
   1 214          YFIT(I)=FUNCTN2(I,B,NTERMS)
   1 215 92       CONTINUE
     216          CALL FCHISQ(Y,WEIGHT,NPTS,NFREE,YFIT,CHISQ)
     217          WRITE(*,*) 'NEW CHISQ AND YFIT FOUND'
     218          WRITE(*,*) 'CHISQ1= ',CHISQ1
     219          WRITE(*,*) 'CHISQ=  ',CHISQ
     220 C
     221          DIFF=DABS((CHISQ1-CHISQ)/CHISQ)
     222          IF (CHISQ .GE. CHISQ1) THEN
     223          IF (CHISQ .EQ. CHISQT) GO TO 110
     224          II=II+1
     225          IF (II .EQ. 4) GO TO 110
     226          CHISQT=CHISQ
     227          FLAMDA=FLAMDA*10.
     228          GO TO 71
     229          ELSE
     230          DO 103 J=1,NTERMS
   1 231          A(J)=B(J)
   1 232          SIGMAA(J)=SQRT(ARRAY(J,J)/ALPHA(J,J))
     233 103      CONTINUE
     234          FLAMDA=FLAMDA/10.
     235          ENDIF
     236 C
```

```
D Line# 1     7                          Microsoft FORTRAN77 V3.20 02/84
     237      IF (DIFF .LE. TOL) GO TO 110
     238       IF (ICOUNT .EQ. NITS) GO TO 110
     239       ICOUNT=ICOUNT+1
     240       CHISQ1=CHISQ
     241       GO TO 16
     242 110   CONTINUE
     243 C
     244 C     *SETUP* THE OUTPUT FILES.
     245 C
     246       OPEN(UNIT=1,FILE=FILN2,STATUS='NEW',FORM='FORMATTED')
     247        WRITE(1,550) FILN1,N1,N2
     248        WRITE(1,551) FILN2
     249        WRITE(1,*) 'THE NUMBER OF ITERATIONS IS:',ICOUNT
     250        IC=1
     251        DO 163 I=1,NTERMS-7,4
1    252        A(I+2)=A(I+2)+FLOAT(N1)-1
1    253        WRITE(1,560) IC
1    254        WRITE(1,570) A(I),SIGMAA(I),A(I+1),SIGMAA(I+1),
1    255       $             A(I+2),SIGMAA(I+2),A(I+3),SIGMAA(I+3)
1    256        IC=IC+1
1    257 163    CONTINUE
     258        WRITE(1,*) 'THE NUMBER OF OFFSET COUNTS IS: ',
     259       $  IFIX(A(NTERMS-3)+.5),' +/- ',IFIX(SIGMAA(NTERMS-3)+.5)
     260        WRITE(1,580) CHISQ1,TOL
     261        WRITE(1,*) 'FLAMDA=',FLAMDA
     262        WRITE(1,*) 'C1=',A(NTERMS-2),'+/-',SIGMAA(NTERMS-2)
     263        WRITE(1,*) 'C2=',A(NTERMS-1),'+/-',SIGMAA(NTERMS-1)
     264        A(NTERMS)=A(NTERMS)+N1-1
     265        WRITE(1,*) 'W1=',A(NTERMS),'+/-',SIGMAA(NTERMS)
     266        CLOSE(1)
     267        OPEN(UNIT=1,FILE=FILN3,ACCESS='SEQUENTIAL',
     268       $   STATUS='NEW',FORM='BINARY')
     269        DO 400 I=1,NPTS
1    270        IDUM(I)=IFIX(YFIT(I)+.5)
1    271 400    CONTINUE
     272        WRITE(1) (IDUM(I),I=1,NPTS)
     273        CLOSE(1)
     274 C
     275        WRITE(*,*) 'FLAMDA=',FLAMDA
     276        WRITE(*,*) 'DO AGAIN (Y/N) ?'
     277        READ(*,162) ANS
     278 162    FORMAT(A1)
     279        IF (ANS .EQ. 'Y' .OR. ANS .EQ. 'y') GO TO 7
     280 C
     281 C      WRITE FORMATS:
     282 C
     283 550    FORMAT(' FITTED FILE IS: ',A15,' FROM CHANNEL ',I4,
     284       $ ' TO CHANNEL ',I4,
     285       $ /,' ',' **************',/)
     286 551    FORMAT('0',' PARAMETER FILENAME IS : ',A20,/)
     287 560    FORMAT('0',' RESULTANT PARAMETERS FOR PEAK NO: ',I2,/)
     288 570    FORMAT(' A= ',F11.4,' +/- ',F8.4,' D= ',F11.4,' +/- ',F8.4,
     289       $    /,' ',' FREQUENCY= ',F11.4,' +/- ',F8.4,
     290       $    ' LINEWIDTH= ',F8.4,' +/- ',F7.4,/)
     291 580    FORMAT(' CHISQ= ',D30.17,
     292       $    /,' ','TOLERANCE= ',F10.8,/)
     293 800    STOP
     294        END
```

```
      1 $NOFLOATCALLS
      2 C       Subroutine MATINV to invert a symmetric matrix
      3 C       and find its determinant (from Bevington).
      4 C
      5         SUBROUTINE MATINV(ARRAY,NTERMS,DET)
      6         INTEGER*4 IK,JK
      7         DOUBLE PRECISION APPAY,AMAX,SAVE
      8         DIMENSION ARRAY(29,29),IK(29),JK(29)
      9 10      DET=1.
     10 11      DO 100 K=1,NTERMS
  1  11 C
  1  12 C       FIND THE LAPGEST ELEMENT ARPAY(I,J) IN THE REST OF MATPIX
  1  13 C
  1  14         AMAX=0.
  1  15 21      DO 30 I=K,NTERMS
  2  16         DO 30 J=K,NTERMS
  3  17 23      IF (DABS(AMAX)-DABS(ARRAY(I,J))) 24,24,30
  3  18 24      AMAX=ARRAY(I,J)
  3  19         IK(K)=I
  3  20         JK(K)=J
  3  21 30      CONTINUE
  1  22 C
  1  23 C       INTERCHANGE ROWS AND COLUMNS TO PUT AMAX IN ARRAY(K,K)
  1  24 C
  1  25 31      IF (AMAX) 41,32,41
  1  26 32      DET=0.
  1  27         GO TO 140
  1  28 41      I=IK(K)
  1  29         IF (I-K) 21,51,43
  2  30 43      DO 50 J=1,NTERMS
  2  31         SAVE=ARRAY(K,J)
  2  32         APPAY(K,J)=APRAY(I,J)
  2  33 50      ARRAY(I,J)=-SAVE
  1  34 51      J=JK(K)
  1  35         IF (J-K) 21,61,53
  1  36 53      DO 60 I=1,NTERMS
  2  37         SAVE=ARRAY(I,K)
  2  38         ARRAY(I,K)=ARRAY(I,J)
  2  39 60      ARRAY(I,J)=-SAVE
  1  40 C
  1  41 C       ACCUMULATE ELEMENTS OF INVEPSE MATRIX
  1  42 C
  1  43 61      DO 70 I=1,NTERMS
  2  44         IF (I-K) 63,70,63
  2  45 63      ARRAY(I,K)=-ARRAY(I,K)/AMAX
  2  46 70      CONTINUE
  1  47 71      DO 80 I=1,NTERMS
  2  48         DO 80 J=1,NTERMS
  3  49         IF (I-K) 74,80,74
  3  50 74      IF (J-K) 75,80,75
  3  51 75      ARRAY(I,J)=ARRAY(I,J)+ARRAY(I,K)*ARRAY(K,J)
  3  52 80      CONTINUE
  1  53 81      DO 90 J=1,NTERMS
  2  54         IF (J-K) 83,90,83
  2  55 83      ARRAY(K,J)=ARRAY(K,J)/AMAX
  2  56 90      CONTINUE
  1  57         ARRAY(K,K)=1./AMAX
  1  58 100     DET=DET*AMAX
     59 C
```

D Line# 1 7 Microsoft FORTRAN77 V3.20 02/84

```
      60 C       RESTORE ORDERING OF MATRIX
      61 C
      62 101     DO 130 L=1,NTERMS
      63         K=NTERMS-L+1
1     64         J=IK(K)
1     65         IF (J-K) 111,111,105
1     66 105     DO 110 I=1,NTERMS
2     67         SAVE=ARRAY(I,K)
2     68         ARRAY(I,K)=-ARRAY(I,J)
2     69 110     ARRAY(I,J)=SAVE
1     70 111     I=JK(K)
1     71         IF (I-K) 130,130,113
1     72 113     DO 120 J=1,NTERMS
2     73         SAVE=ARRAY(K,J)
2     74         ARRAY(K,J)=-ARRAY(I,J)
2     75 120     ARRAY(I,J)=SAVE
1     76 130     CONTINUE
      77 140     RETURN
      78         END
```

Name	Type	Offset	P	Class
AMAX	REAL*8	242		
ARRAY	REAL*8	0	*	
DABS				INTRINSIC
DET	REAL	8	*	
I	INTEGER*4	250		
IK	INTEGER*4	2		
J	INTEGER*4	258		
JK	INTEGER*4	118		
K	INTEGER*4	234		
L	INTEGER*4	310		
NTERMS	INTEGER*4	4	*	
SAVE	REAL*8	282		

Name	Type	Size	Class
MATINV			SUBROUTINE

Pass One No Errors Detected
78 Source Lines

```
D Line# 1      7                          Microsoft FORTRAN77 V3.20 02/84
       1 $NOFLOATCALLS
       2 C       Funtion FUNCTN(I,A,NTERMS) is the derivative
       3 C       of the intensity of a laser polarisation spectrum.
       4 C
       5         FUNCTION FUNCTN2(I,A,NTERMS)
       6         INTEGER I,NTERMS
       7         REAL A(29),S,FLOAT
       8 C
       9         FUNCTN2=A(NTERMS-2)*EXP(-1.*(I-A(NTERMS))**2/A(NTERMS-1))
      10      $   *(I-A(NTERMS))+A(NTERMS-3)
      11         DO 10 J=1,NTERMS-7,4
 1    12         S=FLOAT(I)
 1    13         X=(A(J+2)-S)/A(J+3)
 1    14         FUNCTN2=FUNCTN2+(A(J)*(1-X*X)+A(J+1)*X)/(1+X*X)**2.
 1    15 10      CONTINUE
      16         RETURN
      17         END

Name     Type          Offset P Class

A        REAL               4 *
EXP                           INTRINSIC
FLOAT                         INTRINSIC
I        INTEGER*4          0 *
J        INTEGER*4          2
NTERMS   INTEGER*4          8 *
S        REAL              10
X        REAL              14

Name     Type          Size   Class

FUNCTN   REAL                 FUNCTION

 Pass One    No Errors Detected
             17 Source Lines
```

```
D Line#  1      7                          Microsoft FORTRAN77 V3.20 02/84
       1 $NOFLOATCALLS
       2 C       FCHISQ SUBROUTINE TO CALCULATE THE CHI-SQUARE
       3 C       OF THE FITTED FUNCTION FUNCTN(I,A,NTERMS).
       4 C
       5         SUBROUTINE FCHISQ(Y,WEIGHT,NPTS,NFREE,YFIT,CHISQ)
       6         DOUBLE PRECISION WEIGHT(1000),CHISQ
       7         REAL YFIT(1000),FLOAT
       8         INTEGER*4 Y(1000)
       9         INTEGER NPTS,NFREE
      10 C
      11         CHISQ=0
      12         IF (NFREE .LE. 0) GO TO 400
      13         DO 300 I=1,NPTS
1     14         CHISQ=CHISQ+WEIGHT(I)*(FLOAT(Y(I))-YFIT(I))**2
1     15 300     CONTINUE
      16 C
      17         CHISQ=CHISQ/FLOAT(NFREE)
      18 400     RETURN
      19         END

Name    Type          Offset P Class

CHISQ   REAL*8            20 *
FLOAT                        INTRINSIC
I       INTEGER*4          2
NFREE   INTEGER*4         12 *
NPTS    INTEGER*4          8 *
WEIGHT  REAL*8             4 *
Y       INTEGER*4          0 *
YFIT    REAL              16 *


Name    Type           Size   Class

FCHISQ                        SUBROUTINE


Pass One    No Errors Detected
            19 Source Lines
```

References

[Aud 85] Audet D., Spectroscopie de polarisation des isotopes du krypton, Master's thesis, McGill University (1985).

[Bev 69] Bevington P.R., Data reduction and error analysis for physical sciences, McGraw-Hill (1969), p.232.

[Bre 32] Breit G., Rosenthal J.E., The isotope displacement in hyperfine structure, Phys. Rev. 41 (1932) 459.

[Brec 76] Bréchignac C., Gerstenkorn S., Isotope shift measurements in even isotopes of Kr (78,80,82,84,86) by means of laser techniques, J. Phys. B10 (1976) 413.

[Broa 74] Broadhurst J.H., Cage M.E., Clark D.L., Greenlees G.W., Griffith J.A., Isaak G.R., High resolution measurements of IS and HFS for ytterbium using a C.W. tunable dye laser, J. Phys. B7 (1974) 1513.

[Broc 66] Brochard J., Vetter R., Méthode de mesure de faibles écarts isotopiques dans des émissions stimulées IR, C.R. Hebd. Seances Acad. Sci. B 265, (1966) 681.

[Cha 78] Champeau R.J., Keller J.C., Spectroscopie laser à très haute résolution sur un jet atomique de Kr, J. Phys. B 11 (1978) 391.

[Dem 81a] Demtroder W., Laser Spectroscopy, Springer (1981), p.89.

[Dem 81b] Demtroder W., ibidem., p.376-442.

[Dem 81c] Demtroder W., ibidem., p.462-546.

[Dem 81d] Demtroder W., ibidem., p.27-30.

[Dem 81e] Demtroder W., ibidem., p.29.

[Ehr 22] Ehrenfest P., The difference between series spectra of isotopes, Nature 109 (1922) 745.

[Ger 77] Gerhardt H., Wenz R., Matthias E., Isotope shifts of the 557 nm transition in even krypton isotopes, Phys. Lett. 61A (1977) 377.

[Ger 79] Gerhardt H., Matthias E., Rinneberg H., Schneider F., Timmermann A., Wenz R., West P.J., Changes in mean square charge radii of stable krypton isotopes, Z. Physik A292 (1979) 7.

[Hal 85] Halo Graphics, Media cybernetics (1985).

[Jac 38] Jackson D.A., Kuhn H., Hyperfine structure, Zeeman effect and isotope shift in the resonance lines of potassium, Proc. R. Soc. London A165 (1938) 303.

[Jac 77] Jackson D.A., Hyperfine structure in the arc spectrum of Kr^{83}, J. Opt. Soc. Am. 67 (1977) 1638.

[Jac 78] Jackson D.A., Isotope shifts in the near IR lines of the arc spectrum of krypton, J. Opt. Soc. Am. 69 (1978) 503.

[Jac 80] Jackson D.A., Isotope shifts in the visible lines of the arc spectrum of krypton, J. Opt. Soc. Am. 70 (1980) 1139.

[Kin 84a] King W.H., Isotope shifts in atomic spectra, Plenum Press (1984), p.6.

[Kin 84b] King W.H., ibidem., p.63-69.

[Klu 77] Kluge H.J., Atomic spectroscopy on short lived isotopes, conference reprint (1977).

[Koc 49] Koch. J., Rasmussen E., Hyperfine structure and nuclear spin of Kr^{83} with seperated isotopes, Phys. Rev. 76 (1949) 1417.

[Mar 86] Maruhn J.A., Hamilton J.H., Exotic atomic nuclei, Scientific American 255 (1986) 80.

[Mic 1893] Michelson A.A., Comparison of the International Meter with the wavelength of the light of cadmium, Astron. Astrophys. 12 (1893) 556.

[Pin 86] Pinard J., private communication (1986).

[Sav 85] Savard G., Spectroscopie de saturation des isotopes du krypton, Master's thesis, McGill University (1985).

[Tee 77] Teets R.E., Kowalski F.V., Hill W.T., Carlson N., Hansch T.W., Laser polarisation spectroscopy, SPIE 113 Laser Spectroscopy (1977) 80.